A genome-wide CRISPR screen identifies UFMylation and TRAMP-like complexes as host factors required for hepatitis A virus infection

Jessie Kulsuptrakul[1], Ruofan Wang[1], Nathan L. Meyers[2], Melanie Ott[2], Andreas S. Puschnik[1,*]

[1] Chan Zuckerberg Biohub, San Francisco, United States

[2] Gladstone Institute of Virology, University of California San Francisco, San Francisco, United States

For correspondence: andreas.puschnik@czbiohub.org

Abstract

Hepatitis A virus (HAV) is a positive-sense RNA virus causing acute inflammation of the liver. Here, using a genome-scale CRISPR screen in a human hepatocyte cell line, we provide a comprehensive picture of the cellular factors, which are exploited by HAV during replication. We identified genes involved in sialic acid biosynthesis and members of the eukaryotic translation initiation factor complex, corroborating their putative roles in HAV infection. Additionally, we uncovered all components of the cellular machinery for UFMylation, a ubiquitin-like protein modification. We showed that HAV translation specifically depends on UFM1 conjugation of the ribosomal protein RPL26. Furthermore, we found that components related to the yeast Trf4/5–Air1/2–Mtr4 polyadenylation (TRAMP) complex, are required for viral translation, independent of controlling HAV poly(A) tails. While the identified HAV host factors were largely distinct compared to other picornaviruses, we highlighted a surprising co-dependency of HAV and hepatitis B virus (HBV) on the TRAMP-like complex. Finally, we demonstrated that

23 pharmacological inhibition of the TRAMP-like complex decreased HAV replication in hepatocyte
24 cells and human liver organoids, thus providing a strategy for host-directed therapy of HAV
25 infection.
26
27 **Introduction**
28 Hepatitis A virus (HAV) is a single-stranded, positive-sense RNA virus and a hepatotropic member
29 of the *Picornaviridae*. Despite successes in vaccine development, HAV remains a common cause
30 of enterically transmitted hepatitis globally, responsible for epidemics in developing and
31 developed countries, and with symptoms ranging from mild inflammation and jaundice to acute
32 liver failure (CDC, 2019; Jacobsen, 2018). However, no specific antiviral treatment is currently
33 available. Thus, a better understanding of the molecular virus-host interactions is important and
34 can provide insights for host-directed therapies.
35 During infection HAV enters host cells through interaction with cell surface molecules,
36 followed by uncoating and delivery of viral RNA from endosomes to the cytosol. The genomic
37 RNA is translated into a polyprotein and subsequently processed into the individual structural
38 and non-structural proteins. HAV then co-opts cellular membranes to form virus-specific
39 organelles, where genome replication occurs. Finally, the newly synthesized genomes are
40 packaged and HAV egresses in the form of quasi-enveloped virions (McKnight and Lemon, 2018).
41 Despite a general understanding of the viral life cycle and suggested roles for certain
42 cellular proteins during infection, a comprehensive assessment and thorough validation of the
43 most critical host factors for HAV infection is lacking. For example, TIM1 (T-cell immunoglobulin
44 mucin receptor 1), also named HAV cellular receptor 1 (HAVCR1), was originally identified as

45 receptor for HAV but a more recent study disproved its essentiality for HAV infection (Das et al.,
46 2017; Kaplan et al., 1996).

47 Additionally, numerous host proteins have been shown to interact with the viral RNA to
48 potentially modulate translation or replication of the HAV genome. For example, the HAV internal
49 ribosome binding site (IRES) is unique in that it requires an intact cellular eukaryotic translation
50 initiation factor complex, while other picornaviruses shut down host mRNA translation by
51 proteolytic cleavage (Ali et al., 2001; Borman and Kean, 1997). Other RNA binding proteins, such
52 as PCBP2 (Poly(RC) binding protein 2), PTBP1 (Polypyrimidine tract-binding protein 1) or La
53 protein have been shown to bind viral RNA, but their importance in viral translation or replication
54 are not fully determined (Gosert et al., 2000; Graff et al., 1998; Jiang et al., 2014).

55 To address these knowledge gaps, we performed a genome-wide CRISPR knockout (KO)
56 screen to identify host cellular factors that are critical for the HAV life cycle in an unbiased
57 fashion. CRISPR screens have successfully been used to study human pathogens, such as
58 mosquito-borne flaviviruses, enteroviruses or hepatitis C virus (HCV) (Diep et al., 2019; Marceau
59 et al., 2016; Zhang et al., 2016).

60 Using this approach, we identified sialic acid and ganglioside biosynthesis genes,
61 important for viral entry, as well as factors of the eukaryotic translation initiation factor complex
62 and PTBP1, previously implicated in HAV translation. Additionally, we uncovered unknown
63 cellular pathways, in particular UFMylation and a TRAMP-like complex (related to the yeast
64 Trf4/5–Air1/2–Mtr4 polyadenylation complex), and pinpoint their role to HAV protein synthesis.
65 Importantly, we demonstrate that these host factor requirements are unique to HAV compared
66 to other picornaviruses. Surprisingly, we reveal that hepatitis B virus (HBV), a DNA virus with a

67 vastly different replication strategy, also strongly depends on ZCCHC14, thus highlighting an
68 unexpected convergence across different viral families to co-opt the same cellular complex.
69 Finally, we provide proof-of-concept for host-directed therapy of HAV infections using a small
70 molecule inhibitor against subunits of the TRAMP-like complex.
71
72 **Results**
73 ***A genome-wide CRISPR screen reveals novel host factors required for HAV infection***
74 To identify host cellular factors that are critical for HAV infection, we conducted a genome-wide
75 CRISPR KO screen in the human hepatocyte cell line Huh7.5.1 using the cytopathic HAV
76 HM175/18f strain (Lemon et al., 1991) (Figure 1A). Infection led to notable cell death after 3 days
77 and surviving cells were collected after 12 days for analysis. We found enrichment of guide RNA
78 (gRNA) sequences targeting genes involved in several pathways known to be required for HAV
79 replication (Figure 1B and Table S1). For example, sialic acid and ganglioside biosynthesis genes
80 (*GNE, CMAS, SLC35A1, UGCG, ST3GAL5*) were recently described to express endosomal receptors
81 for HAV and other viruses (Baggen et al., 2016; Das et al., 2020; Ding et al., 2018; Drake et al.,
82 2017; Han et al., 2018). We also identified *PTBP1* and members of the eukaryotic translation
83 initiation factor complex (*EIF4B, EIF3C, EIF3CL*), which have known roles in IRES-mediated
84 translation of HAV and other picornaviruses (Avanzino et al., 2017; Borman and Kean, 1997;
85 Gosert et al., 2000; Pestova et al., 1996). The highly enriched VPS4A is an AAA-ATPase that
86 regulates endosomal sorting complexes required for transport (ESCRT), important for budding of
87 several enveloped viruses as well as egress of HAV (Feng et al., 2013; Votteler and Sundquist,

88 2013). Together, the identification of host components previously implicated in HAV infection
89 validates the phenotypic selection in our CRISPR screen.

90 Importantly, gene ontology (GO) analysis of enriched genes (RIGER p-value < 0.001)
91 revealed additional pathways, which have not previously been linked to HAV infection (Figure 1C,
92 Table S2). First, we identified all known components of the machinery for UFMylation (*UFM1,*
93 *UBA5, UFL1, UFC1, UFSP2*), a ubiquitin-like protein modification (Gerakis et al., 2019; Komatsu et
94 al., 2004) (Figures 1B and 1C). Second, the two related non-canonical poly(A) RNA polymerases,
95 PAPD5 (also known as TENT4B or TRF4-2) and PAPD7 (also known as TENT4A or TRF4-1) were
96 notably enriched (Figures 1B and 1C) (Warkocki et al., 2018). Finally, ZCCHC14 (Zinc Finger CCHC
97 Domain-Containing Protein 14), the second most enriched gene, has been shown to associate
98 with PAPD7 (Figure 1B) (Go et al., 2019). Together, these proteins form a TRAMP-like complex,
99 generally containing an RNA polymerase and zinc finger protein, and are likely to play a critical
100 role in HAV infection (Hamill et al., 2010; Lubas et al., 2011).

101 To assess the specificity of the identified cell components across different viral infections,
102 we systematically compared our hits with CRISPR screens for host factors of human rhinovirus
103 C15 (HRV-C15) and enterovirus D68 (EV-D68), two distantly related picornaviruses (Diep et al.,
104 2019). Despite differences in tissue tropism and pathogenesis, HAV shares common replication
105 strategies with other members of the *Picornaviridae* family to translate and synthesize its
106 genomes. However, other than sialic acid biosynthesis genes among the EV-D68 hits, there were
107 no commonalities, indicating divergent evolution of host factor dependencies (Figures S1A and
108 S1B). Next, we compared our results to a CRISPR screen for hepatitis C virus (HCV) infection,

109 another hepatotropic positive-sense RNA virus (and member of the *Flaviviridae* family) but found
110 no overlap in the host factor requirements (Figure S1C) (Marceau et al., 2016).
111 Lastly, a comparison with results from a CRISPR screen for hepatitis B virus (HBV), a DNA
112 virus replicating through reverse transcription, surprisingly highlighted ZCCHC14 as a shared host
113 dependency factor between HAV and HBV (Figure S1D) (Hyrina et al., 2019). Together, these data
114 illustrate that the host factor requirements for HAV are largely unique compared to other
115 picornaviruses but reveal an unexpected commonality between HAV and HBV infection.
116
117 ***Knockout of identified host factor genes impairs HAV replication***
118 To validate the results of our screen, we generated isogenic KO cell lines in several genes by
119 CRISPR-Cas9 gene editing resulting in loss of protein expression (Figures S2A-C). Upon HAV
120 infection, we observed significant reduction of both viral replication and particle production
121 (ranging from 10-1,000 fold) relative to levels in wild-type (WT) cells at 72 hours post-infection
122 (hpi) (Figures 2A and S3). As PAPD5 and PAPD7 are both human orthologues of yeast Trf4p and
123 display partial redundancy in their polyadenylation function (Warkocki et al., 2018), we
124 generated *PAPD5/PAPD7* double knockout (DKO) cell lines (Figure S2A). We observed a
125 significantly stronger reduction in viral replication in the DKO cells compared to the single *PAPD5*
126 or *PAPD7* KO cells underscoring their redundant activity for HAV replication (Figure 2B). To assess
127 viral growth phenotypes over time, we performed an infection assay using a recombinant
128 reporter virus that expresses nanoluciferase from within its polyprotein (HAV-NLuc). We
129 measured a ~10^4 fold increase in luminescence in WT cells after 72hpi but there was striking
130 attenuation of luciferase expression in host factor KO lines, highlighting that the growth defect

131 persists through multiple replication cycles (Figure 2C). Importantly, when we complemented
132 *UBA5*, *PAPD5* and *ZCCHC14* KO cells with the respective cDNAs, we observed a significant
133 increase in HAV replication (Figures 2D-F and S2C).

134 It is of note that our screen did not reveal HAVCR1 (TIM1) as an essential host factor for
135 HAV infection. To address this further, we performed a viral attachment and internalization assay
136 in isogenic *HAVCR1* KO cells. We only observed a minor defect of internalized viral RNA at 6hpi
137 and viral RNA levels were only reduced by ~2 fold relative to WT cells at 30hpi (Figure S4). By
138 contrast, in *SLC35A1* KO cells intracellular viral RNA was decreased by ~80% at 6hpi and ~95% at
139 30hpi. We conclude that *HAVCR1* is not essential for the HAV life cycle, while sialic acid
140 biosynthesis is critical for viral entry and establishing infection. Overall, the genetic knockout
141 studies confirm that the CRISPR screen identified genes with robust roles in the HAV life cycle.

142 Finally, we confirmed the finding from the comparative CRISPR screen analysis that the
143 newly implicated UFMylation machinery and TRAMP-like complexes are distinct to HAV among
144 different *Picornaviridae* members. HAV RNA levels were greatly reduced while enterovirus 71
145 (EV-71) and encephalomyocarditis virus (EMCV) RNA levels were not affected in *UFM1* KO cells
146 (Figure 2G). Interestingly, human rhinovirus A2 (RV-A2) replication was increased suggesting that
147 UFMylation can mediate pro- and antiviral functions in host cells, depending on the virus species.
148 Similarly, in cells deficient in both PAPD5 and PAPD7, HAV RNA levels were severely and EMCV
149 RNA levels moderately decreased while EV-71 and RV-A2 replication were unaffected (Figure 2H).
150 Together, these data confirm that the genes identified by the CRISPR screen have important and
151 distinct functions in the HAV life cycle but not for other picornaviruses.

152

153 ***HAV depends on UFMylation of the ribosomal protein RPL26 for efficient translation***

154 Struck by the unique dependency of HAV on UFMylation and no described role in viral infection,
155 we first followed up on this cellular pathway. *UFM1* encodes the 85 amino acid long ubiquitin-
156 fold modifier 1, which acts as a protein modification and is conserved among most eukaryotes
157 except for yeast and other fungi (Komatsu et al., 2004). Like ubiquitination, UFM1 is covalently
158 attached to its targets following an E1–E2–E3 reaction consisting of the UFM1-activating enzyme
159 UBA5, the UFM1-conjugating enzyme UFC1 and the UFM1-specific ligase UFL1 (Figure 3A)
160 (Komatsu et al., 2004; Tatsumi et al., 2010). Usually, UFM1 is present in a precursor form, which
161 first requires cleavage of the last two C-terminal amino acids by the UFM1-specific protease
162 UFSP2 to expose Gly at position 83 (Komatsu et al., 2004). UFSP2 also operates as the major de-
163 UFMylation enzyme, removing UFM1 molecules from their targets (Kang et al., 2007). Our screen
164 identified all known components of the UFMylation machinery including the additionally
165 associated proteins DDRGK1 and ODR4 (encoded by *C1orf27*) (Figure 3A) (Chen et al., 2014; Wu
166 et al., 2010). WT cells contain free UFM1 as well as conjugated UFM1 as detected by immunoblot
167 (Figure 3B). To probe whether functional conjugation of UFM1 is required for HAV infection, we
168 mutated different components of the pathway. Deletion of UBA5 led to an absence of conjugated
169 UFM1, while UFSP2 KO resulted in hyper-conjugation, consistent with their reported activities
170 (Figure 3B). Both conditions led to a stark reduction of viral RNA in infected cells, suggesting that
171 the modification needs to be reversible for its proviral function (Figure 3C). Moreover, we
172 reconstituted *UFM1* KO cells with WT UFM1, a more stable Gly83Ala UFM1 modification or ΔC3
173 UFM1, which lacks the last 3 C-terminal amino acids essential for conjugation (Figure 3B)
174 (Komatsu et al., 2004). Complementation with WT UFM1 and Gly83Ala UFM1 significantly

175 restored HAV replication (Figure 3C). By contrast, conjugation-deficient ΔC3 UFM1 did not rescue
176 viral infection. Consistent with this, complementation of *UBA5* KO cells with WT UBA5 but not
177 catalytically inactive enzyme also restored UFM1 conjugation and viral replication (Figures 3B and
178 S5). Together, these data establish that functional and reversible UFM1 conjugation is critical for
179 HAV replication.

180 Next, in order to assess whether the defect occurs during early viral translation or later
181 during the genome replication step, we used HAV replicon RNA expressing firefly luciferase (Fluc).
182 We detected a marked defect in *UBA5* and *UFSP2* KO cells within 10h post-electroporation
183 (Figure 3D). To specifically measure the effect on translation of incoming viral RNA, we used a
184 replication-incompetent replicon (containing a GDD→GAA mutation in the viral polymerase) and
185 observed strongly reduced luciferase expression in both KO cells (Figures 3E and S6A). We
186 excluded that observed phenotypes were due to differences in cell viability or proliferation post-
187 electroporation (Figure S6B). We therefore conclude that UFMylation is required for optimal
188 translation of HAV RNA.

189 Recently, the ribosomal protein RPL26 was identified as a major target for UFMylation in
190 human cells (Walczak et al., 2019; Wang et al., 2019). Thus, we tested whether UFMylated RPL26
191 is important for efficient HAV translation. Consistent with previous findings, we detected
192 modified RPL26 at the molecular weight corresponding to UFM1 conjugates (Figure 3F).
193 Interestingly, only a small fraction of RPL26 is UFMylated and the conjugation appears transient
194 as it can only be visualized in *UFSP2* KO cells, which lack de-UFMylation activity. It was further
195 shown that conjugation of UFM1 occurs at C-terminal lysines of RPL26 (Walczak et al., 2019;
196 Wang et al., 2019). We generated cell lines with ectopic WT RPL26 or cDNA containing five lysine

197 to arginine mutations ("5KR RPL26") and confirmed that ectopic 5KR RPL26 was not UFMylated
198 (Figures 3G and S7A). HAV infection of WT Huh7.5.1 cells expressing 5KR RPL26 was reduced
199 compared to cells containing ectopic WT RPL26, which largely phenocopied the *UFM1* KO effect
200 (Figure 3H). By contrast, there was no dominant negative effect of 5KR RPL26 in transduced *UFM1*
201 or *UFSP2* KO cells, where HAV replication was already fully reduced compared to WT Huh7.5.1
202 containing WT RPL26 (Figure 3H). Similarly, we measured reduced HAV RNA levels in previously
203 characterized U2OS cells expressing 5KR RPL26 and a CRISPRi system to knockdown endogenous
204 WT RPL26 (Walczak et al., 2019) (Figure S7B). Lastly, 5KR RPL26 cells exhibited increased RV-A2
205 infection (Figure S7C), thus mirroring the effect of *UFM1* deletion (Figure 2G). Together, the
206 results indicate that UFM1 and RPL26 are functionally linked and support a model where HAV
207 requires active UFMylation of RPL26 for translation.
208
209 ***TRAMP-like complexes support HAV translation independent of polyadenylation of HAV tails***
210 Intrigued by the strong phenotypes on HAV replication and a critical role in the life cycles of both
211 HAV and HBV, we performed mechanistic studies on the TRAMP-like complex components
212 PAPD5, PAPD7 and ZCCHC14. The two non-canonical poly(A) RNA polymerases PAPD5 and PAPD7
213 can transfer poly or oligo(A) to a variety of RNA substrates (e.g. mRNAs, miRNAs, snoRNAs and
214 rRNAs) in a template-independent manner (Berndt et al., 2012; Boele et al., 2014; Rammelt et
215 al., 2011; Shcherbik et al., 2010; Shin et al., 2017). Their cellular activities include stabilization of
216 mRNAs for translation as well as specifying different RNA species for turnover by the exosome
217 complex (Lubas et al., 2011; Vaňáčová et al., 2005; Warkocki et al., 2018). Recently, ZCCHC14 has
218 been shown to interact with PAPD5 and PAPD7 to support HBV infection (Hyrina et al., 2019) and

219 consistent with that we observed strong reduction of HBV RNA levels in *ZCCHC14* KO cells (Figure
220 S8A).

221 To determine the function of the TRAMP-like complex during HAV infection, we first
222 measured the effects of *PAPD5/7* DKO or *ZCCHC14* KO on viral translation and replication using
223 viral replicon RNA. We observed a notable defect in luciferase expression immediately post-
224 electroporation, suggesting inefficient translation of viral RNA (Figure 4A). While WT cells
225 supported replicon replication at later timepoints, luminescence decayed in the KO cells. We
226 additionally probed viral translation directly using the replication-incompetent HAV replicon and
227 observed drastically reduced luciferase expression from incoming RNA immediately post-
228 electroporation in DKO and *ZCCHC14* KO cells (Figures 4B). By contrast, translation of
229 electroporated firefly mRNA was not affected, excluding a general translation defect in KO cells
230 (Figure S8B). As translation from viral RNA is directly linked to RNA stability, we measured HAV
231 RNA levels upon infection over time. However, we did not detect differences in viral RNA levels
232 between WT, DKO or *ZCCHC14* KO cells early during infection (Figure 4C). We therefore conclude
233 that deletion of TRAMP-complex components affects HAV translation but not HAV RNA stability.

234 For HBV, mechanistic studies revealed that HBV surface antigen expression requires RNA
235 tailing by TRAMP-like complexes (Hyrina et al., 2019). As HAV has a polyadenylated genome and
236 longer poly(A) tails can promote translation (Bergamini et al., 2000), we assessed the length
237 distribution of HAV poly(A) tails from infected WT and KO cells by polyacrylamide gel
238 electrophoresis but we did not observe a notable difference (Figure 4D). By contrast, HBV tails
239 were reduced in *ZCCHC14* KO cells, confirming the expected defect (Figure 4D). To corroborate
240 that HAV tail length is not affected, we performed TOPO cloning followed by Sanger sequencing

241 as well as a higher resolution electrophoretic shift assay using TapeStation, confirming that HAV
242 tails are not shortened in KO cells (Figures 4E and S8C).

243 To explore a different function of PAPD5 and PAPD7 for HAV infection, we looked at the
244 composition of viral poly(A) tails. Recently, it was shown that PAPD5 and PAPD7 can introduce
245 guanosines at low frequencies into poly(A) tails resulting in increased stability against CCR4-NOT
246 dependent deadenylation (Lim et al., 2018). However, we did not observe an elevated frequency
247 of non-adenosine nucleotides in WT vs DKO cells within HAV poly(A) tails (Figure 4F). Rather,
248 almost all analyzed tails exclusively consisted of adenosines in both conditions. Together, the
249 data suggest that TRAMP-like complexes do not support viral translation by regulating the length
250 or composition of HAV poly(A) tails.

251 As the described cellular functions of PAPD5 and PAPD7 depend on their catalytic activity,
252 we complemented KO or DKO cells with WT or catalytically inactive (CAT) (containing two
253 aspartate to alanine substitutions in the active site) cDNAs (Figure S2C) (Rammelt et al., 2011).
254 Importantly, infection of the complemented cell lines established that the catalytic activities of
255 PAPD5 and PAPD7 are required to support viral replication (Figures 4G and S8D). We speculate
256 that the TRAMP-like complex either modulates HAV RNA in a (so far) unrecognized manner or
257 that expression of a cellular protein, which is critical for HAV translation, depends on
258 polyadenylation of its transcript. In conclusion, we find that the catalytic activity is required to
259 support viral translation, independent of directly modulating viral poly(A) tails or RNA stability.

260

261

262 ***Pharmacological Inhibition of PAPD5 and PAPD7 exhibits an antiviral effect against HAV***
263 ***infection***

264 As the enzymatic function of PAPD5 and PAPD7 are required for HAV infection, we explored
265 whether pharmacological inhibition has an antiviral effect. We used RG7834 (Figure 5A), a small
266 molecule compound belonging to the chemical class of the dihydroquinolizinones. Interestingly,
267 this compound was first identified as a potent inhibitor for HBV surface antigen secretion
268 (Mueller et al., 2018), and PAPD5 and PAPD7 were subsequently shown to be its cellular targets
269 (Mueller et al., 2019).

270 To test whether RG7834 also exhibits activity against HAV replication, we performed a
271 dose-response curve and calculated a 50% effective concentration (EC_{50}) of 12.76 nM for
272 inhibition of HAV replication (Figure 5B). This is far below the measured 50% cytotoxic
273 concentration (CC_{50}) of >10 µM (Figure S9A). Drug treatment of infected *PAPD5* or *PAPD7* KO
274 cells suggested that RG7834 has a stronger inhibitory effect on the PAPD5 activity as reduction
275 of viral RNA is more substantial in the *PAPD7* KO+RG7834 condition (Figure S9B). Intrigued by the
276 fact that RG7834 inhibits both HAV and HBV, we also measured the effects on two additional
277 liver-specific viruses, HCV and hepatitis E virus (HEV). However, RG7834 only showed significant
278 reduction of HAV and HBV RNA levels (Figure 5C-F). This is consistent with the comparative
279 CRISPR screen analysis for HCV as well as unchanged viral replication levels in DKO cells for both
280 HCV and HEV (Figure S9C).

281 Finally, we performed infection assays in human liver organoid cultures (Broutier et al.,
282 2016). We observed significant dose-dependent reduction of HAV RNA in both stem cell-like and
283 differentiated organoids under RG7834 treatment (Figures 5G and S9D). Together, our results

284 demonstrate that pharmacological inhibition of PAPD5/7 is a promising strategy for host-directed
285 therapy of HAV infection.
286
287 **Discussion**
288 This study provides a comprehensive assessment of the host factors that are critical for HAV
289 infection. The identified genes comprise several cellular pathways and complexes, such as sialic
290 acid biosynthesis, eukaryotic translation initiation, UFMylation, TRAMP-like complexes and
291 others. We corroborated that the putative HAV receptor, HAVCR1, is not essential for infection.
292 Rather, we found multiple genes linked to sialic acid and ganglioside biosynthesis, which are
293 important for efficient HAV uptake (Das et al., 2020). The screen also identified eukaryotic
294 translation initiation factor components and PTBP1, which were previously linked to HAV
295 translation (Avanzino et al., 2017; Borman and Kean, 1997; Gosert et al., 2000; Pestova et al.,
296 1996).
297 Importantly, we revealed two cellular pathways, UFMylation and TRAMP-like complexes,
298 which had not been implicated in HAV life cycle before. UFMylation is a ubiquitin-like, post-
299 translation modification. We demonstrated that HAV specifically depends on UFMylation of the
300 ribosomal protein RPL26 for efficient translation. The cellular function of this protein
301 modification is still an emerging field of research but it has been linked to the regulation of the
302 ER stress response and ribosome-associated quality control (Walczak et al., 2019; Wang et al.,
303 2019). Specific ribosomal or ribosome-associated proteins have been shown to be required for
304 efficient translation of other viral genomes (Landry et al., 2009; Majzoub et al., 2014). RPL26 is
305 located near the ribosome exit tunnel and its modification could facilitate dynamic and reversible

306 conformation changes to improve translation of specific amino acid sequences or resolve certain
307 secondary structure in the RNA as suggested by the requirement for active UFMylation and de-
308 UFMylation during HAV infection. Additional studies, such as biochemical analysis and ribosome
309 profiling of the different ribosomal subpopulations, are needed to gain a better understanding
310 of its role during translation of viral and cellular mRNAs. The contrasting phenotypes observed
311 during HAV and RV-A2 infection in *UFM1* KO cells may also be utilized as tools for future studies
312 of the molecular effects of UFMylation.

313 Furthermore, we identified the TRAMP-like complex components ZCCHC14, PAPD5 and
314 PAPD7 and demonstrated that they are required for HAV translation. PAPD5 and PAPD7 have
315 been described to possess polyadenylation activity as well as the ability to generate mixed tails
316 (Lim et al., 2018; Warkocki et al., 2018). Despite showing that their catalytic activity is required
317 to support HAV infection, we did not observe any abnormalities in HAV poly(A) tail length,
318 composition or viral RNA stability in TRAMP-like complex deficient cells. However, this is
319 consistent with previous observations that picornavirus polyadenylation is template-dependent,
320 for example by the presence of a homotypic poly(U) sequence in the picornavirus negative-sense
321 RNA (Spector and Baltimore, 1975). Moreover, studies using poliovirus, another picornavirus,
322 suggested that the picornaviral RNA-dependent RNA polymerase uses reiterative transcription as
323 it replicates the poly(A) tails of viral RNA (Kempf et al., 2013; Steil et al., 2010). These findings
324 support that PAPD5 and PAPD7 are not necessarily required for HAV poly(A) tail generation or
325 maintenance. Thus, the TRAMP-like complex may fulfill other functions, for example by directly
326 regulating viral translation. In studies using *C. elegans*, deletion of the worm orthologs of PAPD5
327 (gld-4) and ZCCHC14 (gls-1) led to reduced polysome formation but did not affect global poly(A)

328 tail lengths, providing evidence of polyadenylation-independent functions of TRAMP-like
329 complexes (Nousch et al., 2014). Alternatively, PAPD5 and PAPD7 could regulate the expression
330 of another host factor critical for HAV translation through RNA tailing.

331 Interestingly, other tested picornaviruses were not dependent on UFMylation or the
332 TRAMP-like complex for efficient translation. Therefore, our data suggests that HAV translation
333 differs even more substantially from other picornaviruses than previously recognized. While it is
334 known that HAV is distinct in its dependency on the cellular eukaryotic translation initiation factor
335 complex (Borman and Kean, 1997), we additionally revealed an unique requirement of
336 UFMylation and the TRAMP-like complex for HAV.

337 Surprisingly though, PAPD5, PAPD7 and ZCCHC14 were identified as critical factors for
338 infection with HBV, a hepatotropic DNA virus with a vastly different life cycle, using chemical and
339 genetic screens (Hyrina et al., 2019; Mueller et al., 2019). Mechanistically, the TRAMP-like
340 complex plays an important role in HBV surface antigen expression by poly(A) tail extension of
341 HBV mRNAs (Hyrina et al., 2019). This highlights a remarkable convergence of two unrelated
342 hepatitis viruses to co-opt the same cellular complex in different ways.

343 Finally, based on these molecular insights, we provided proof-of-concept that
344 pharmacological inhibition of PAPD5 and PAPD7 decreases infection levels of HAV and HBV. Thus,
345 this study exemplifies that host factor screens are a powerful strategy to gain a comprehensive
346 understanding of the most critical cellular pathways for viral infections, and to illuminate new
347 drug targets, which can be shared across different viral families.

Figure 1

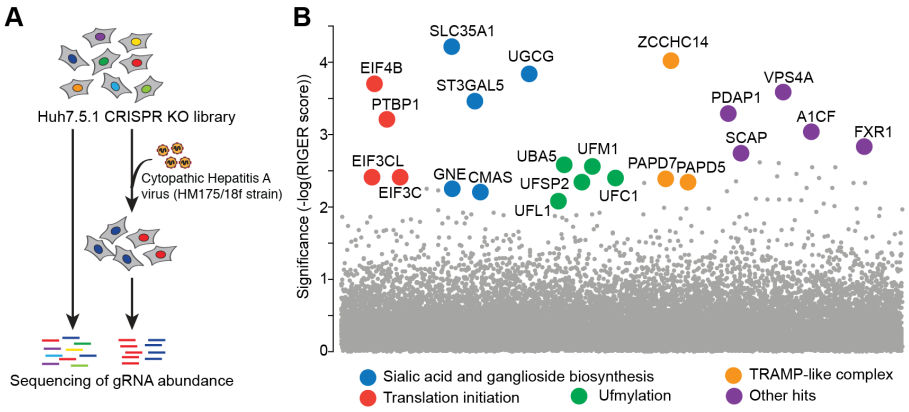

C

GO term	p-value
protein K69-linked ufmylation	9.20E-10
mitochondrial RNA catabolic process	5.09E-07
RNA polyadenylation	4.70E-06
ubiquinone biosynthetic process	2.77E-05
translation initiation factor activity	3.73E-05
TRAMP complex	8.35E-05
Ragulator complex	2.08E-04
N-acetylneuraminate metabolic process	7.53E-04

Figure 1. Genome-wide CRISPR KO screen identifies host cellular factors important for HAV infection. (A) Schematic of the genome-wide CRISPR KO screen. A library of Huh7.5.1 CRISPR-Cas9 cells was infected with cytopathic HAV HM175/18f and virus-resistant cells were harvested 12 days post-infection. gRNA abundance was measured in the original and selected cell population by next-generation sequencing. **(B)** Significance of enriched genes in CRISPR KO screen based on RIGER analysis. Hits were clustered and colored by function. **(C)** Selected terms from gene ontology (GO) analysis of genes enriched in CRISPR KO screen (RIGER p-value < 0.001).

Figure S1

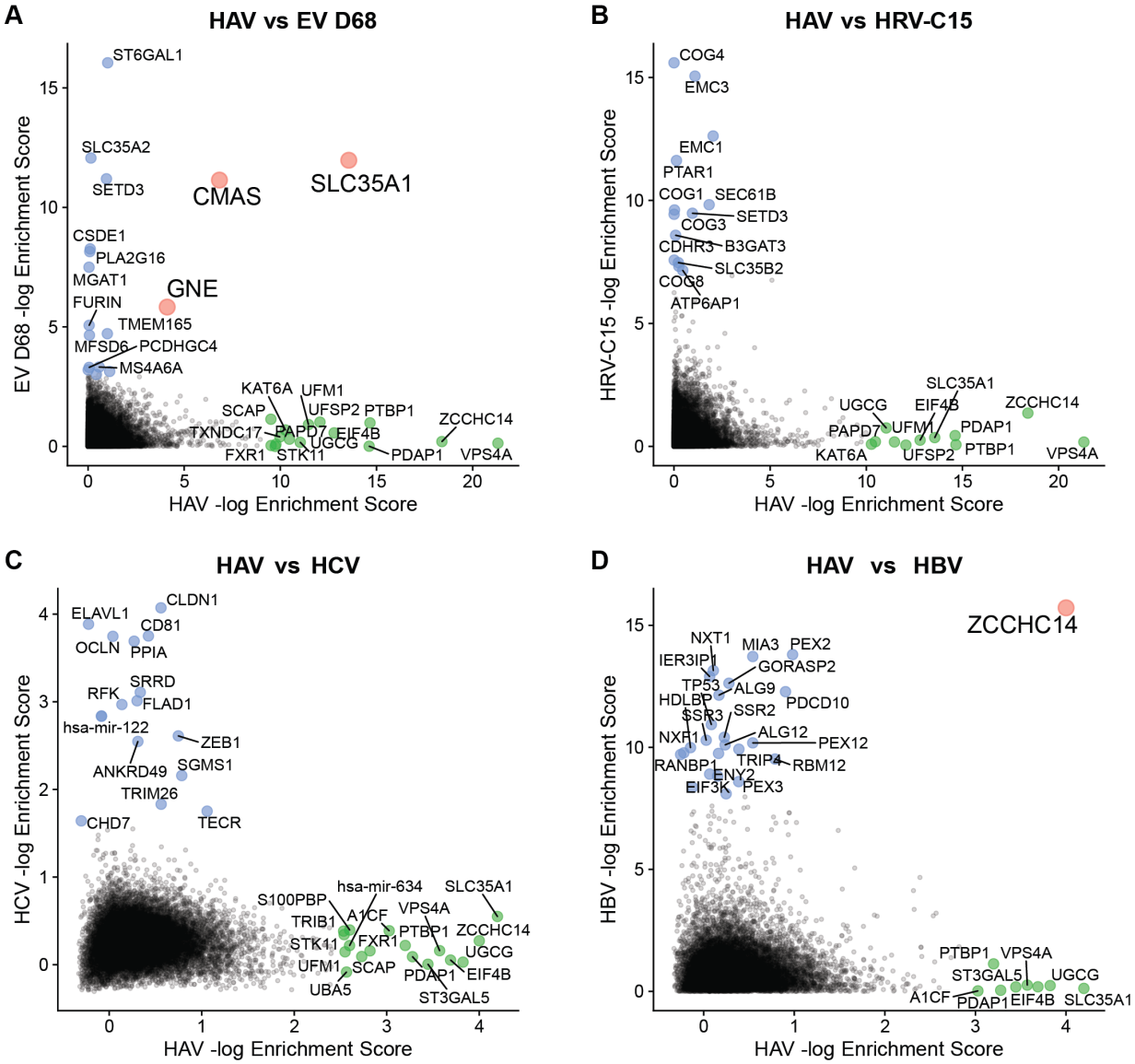

Figure S1. Comparative CRISPR screen analysis reveals that HAV host factors are distinct from other picornaviruses and HCV but highlights that ZCCHC14 is a shared hit between HAV and HBV, Related to Figure 1. Comparison of HAV CRISPR screen gene enrichment scores with hits from **(A)** EV-D68 (Diep et al., 2019), **(B)** HRV-C15 (Diep et al., 2019), **(C)** HCV (Marceau et al., 2016), or **(D)** HBV CRISPR screens (Hyrina et al., 2019). Overlapping hits from both screens are highlighted in red.

Figure 2

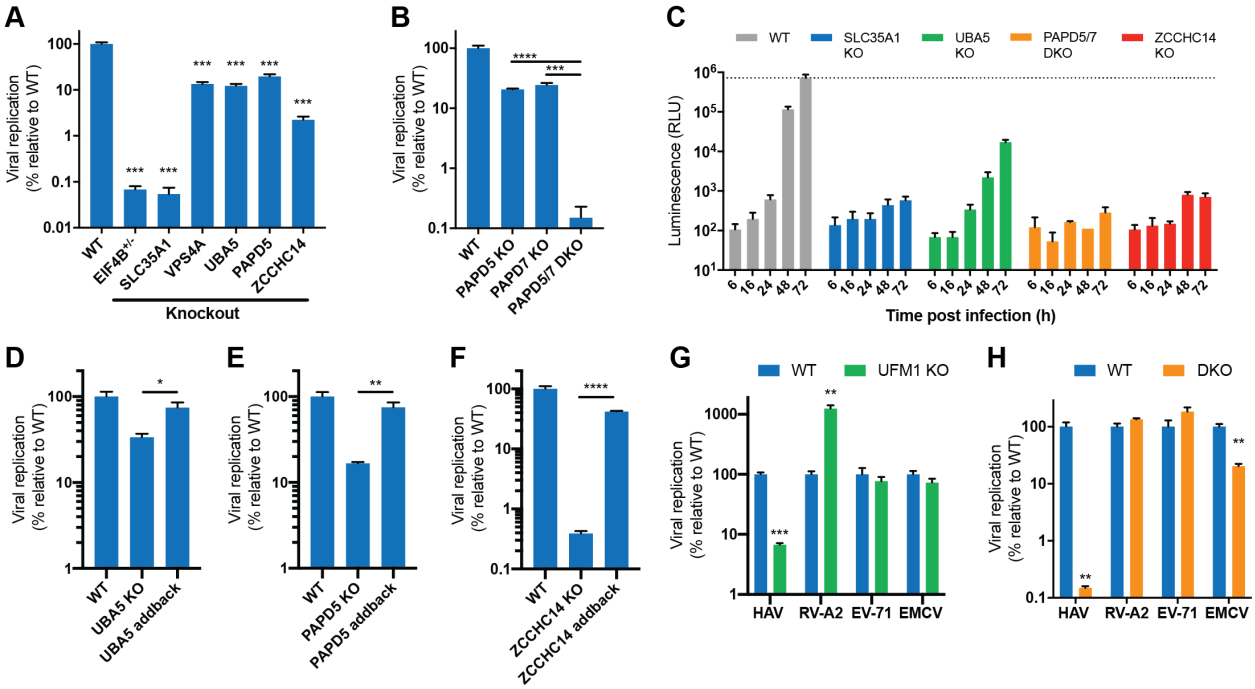

Figure 2. Knockout of identified host factor genes reduces HAV replication. (A) Quantification of HAV RNA in WT and clonal KO cell lines 3 dpi by RT-qPCR. **(B)** Quantification of HAV RNA in WT, *PAPD5* KO, *PAPD7* KO and *PAPD5/PAPD7* double KO (DKO) cells 3 dpi by RT-qPCR. **(C)** Viral growth curves using recombinant HAV expressing nanoluciferase (HAV-Nluc). WT, *SLC35A1* KO, *UBA5* KO, *PAPD5/7* DKO and *ZCCHC14* KO cells were infected, lysed at indicated timepoints and luciferase levels were measured. Dotted line indicates luminescence levels in WT cells at 72 hpi. Data are displayed as means ± s.d. (n=2 biological replicates). **(D-F)** Quantification of HAV RNA in WT, *UBA5* KO (**D**), *PAPD5* KO (**E**), or *ZCCHC14* KO (**F**) cells and KO cells complemented with respective cDNAs 3 dpi by RT-qPCR. **(G-H)** Quantification of HAV, human rhinovirus A2 (RV-A2), enterovirus 71 (EV-71) and encephalomyocarditis virus (EMCV) RNA in WT vs *UFM1* KO cells (**G**) or WT vs DKO cells (**H**) by RT-qPCR. Cells infected with HAV or RV-A2 were harvested after 48h, with EV-71 after 24h and with EMCV after 8h.

377 For all RT-qPCR experiments, viral RNA was normalized to 18S RNA and results are displayed
378 relative to infection in WT cells. Datasets represent means ± s.e.m. (n=3 biological replicates). P
379 values were determined by unpaired two-sided t-tests using GraphPad Prism 8. *, $p<0.05$; **,
380 $p<0.01$; ***, $p<0.001$; ****<0.0001.

Figure S2

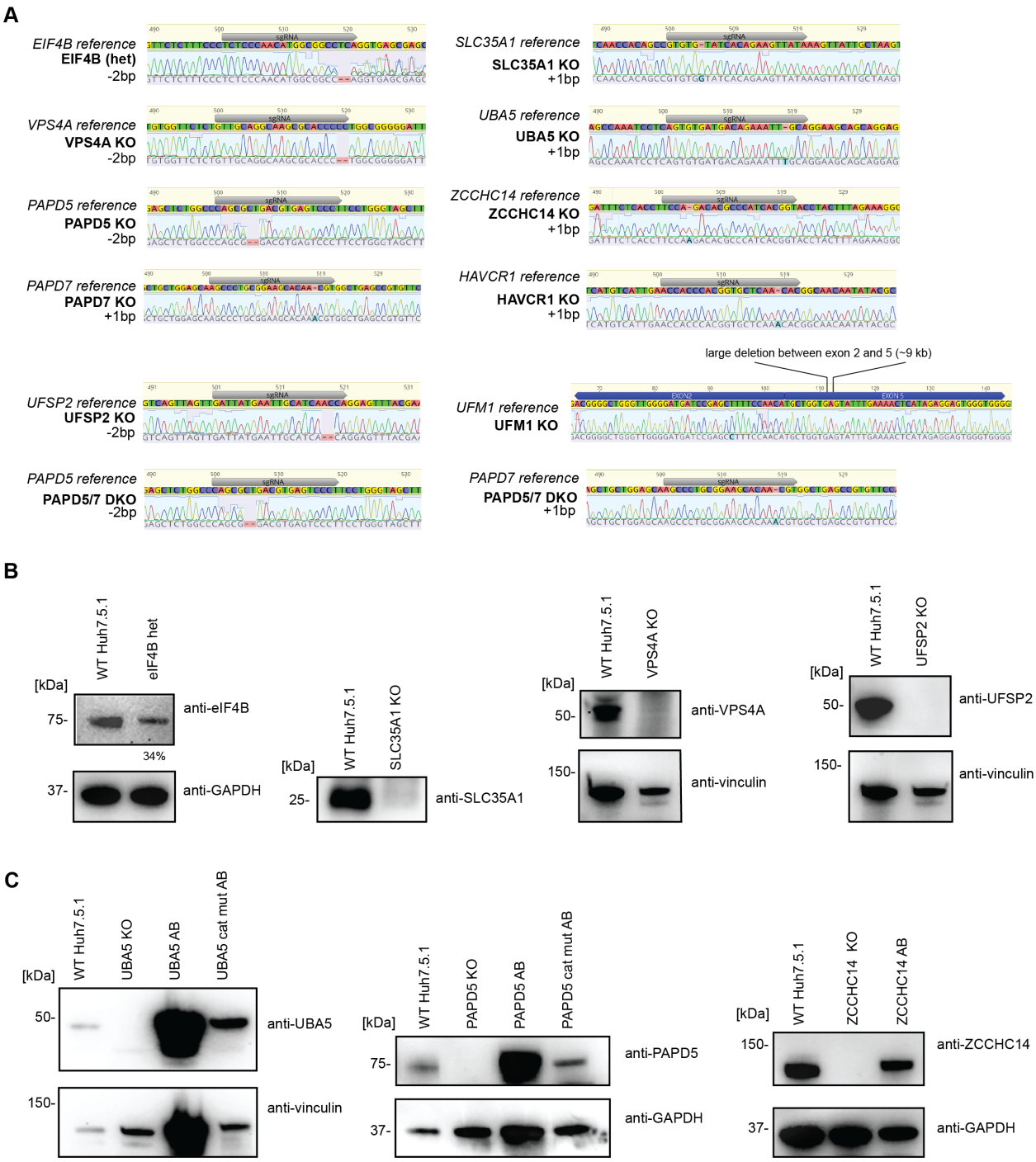

Figure S2. Genotyping and immunoblotting of clonal Huh7.5.1 KO cell lines, Related to Figure 2. (A) Sanger sequencing of gRNA targeted loci of clonal KO cell lines. Traces were aligned to corresponding reference sequences and indel mutations determined. Reads of gRNA targeted

385 PAPD5 and PAPD7 loci in clonal Huh7.5.1 DKO cells are displayed. UFM1 gene was simultaneously
386 targeted by two gRNAs cutting in exon 2 and exon 5 resulting in a large genomic deletion. **(B)**
387 Immunoblots for clonal *eIF4B*, *SLC35A1*, *VPS4A* and *UFSP2* KO cell lines. For eIF4B, a heterozygous
388 clone harboring one allele with a -2bp deletion and one WT allele, quantification of the band (in
389 %) is normalized to GAPDH signal and relative to WT indicating decrease of expression in
390 heterozygous clone. For SLC35A1, WT and KO cells were lysed in RIPA buffer and lysates were
391 immunoprecipitated using anti-SLC35A1 antibody and protein G beads prior to immunoblot.
392 GAPDH and Vinculin were used as loading controls. **(C)** Immunoblots of WT, *UBA5* KO, *PAPD5* KO
393 or *ZCCHC14* KO cells as well as KO cells complemented with respective cDNAs. GAPDH and
394 Vinculin were used as loading controls.

Figure S3

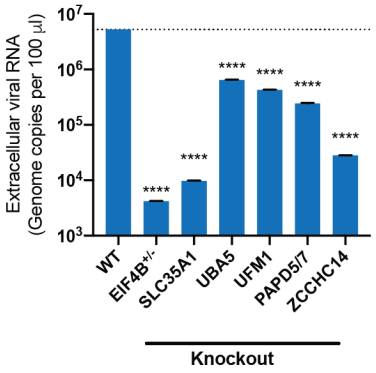

Figure S3. Host factor knockout decreases extracellular viral RNA, Related to Figure 2. Quantification of extracellular viral RNA in supernatant of cells 3 dpi using HM175/18f HAV. RNA was extracted from supernatant, measured by RT-qPCR and compared to a standard curve of in vitro transcribed viral RNA to determine genome copies. Dataset represents means ± s.e.m. (n=2 biological replicates). P values were determined by one-way Anova with uncorrected Fisher's Least Significant Difference test using GraphPad Prism 8. *, $p<0.05$; **, $p<0.01$; ***, $p<0.001$; ****<0.0001.

Figure S4

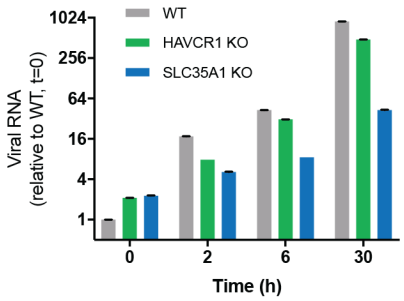

403

404 **Figure S4. Deletion of sialic acid biosynthesis severely impairs viral entry, while *HAVCR1* KO is**

405 **not critical for viral uptake, Related to Figure 2.** Quantification of HAV RNA in WT, *HAVCR1* KO

406 and *SLC35A1* KO cells by RT-qPCR after cells were infected on ice, incubated at 37C, and washed

407 before harvest at indicated times. Viral RNA was normalized to 18S RNA and results are displayed

408 relative to infection in WT cells. Datasets represent means ± s.e.m. (n=3 biological replicates).

409

Figure 3

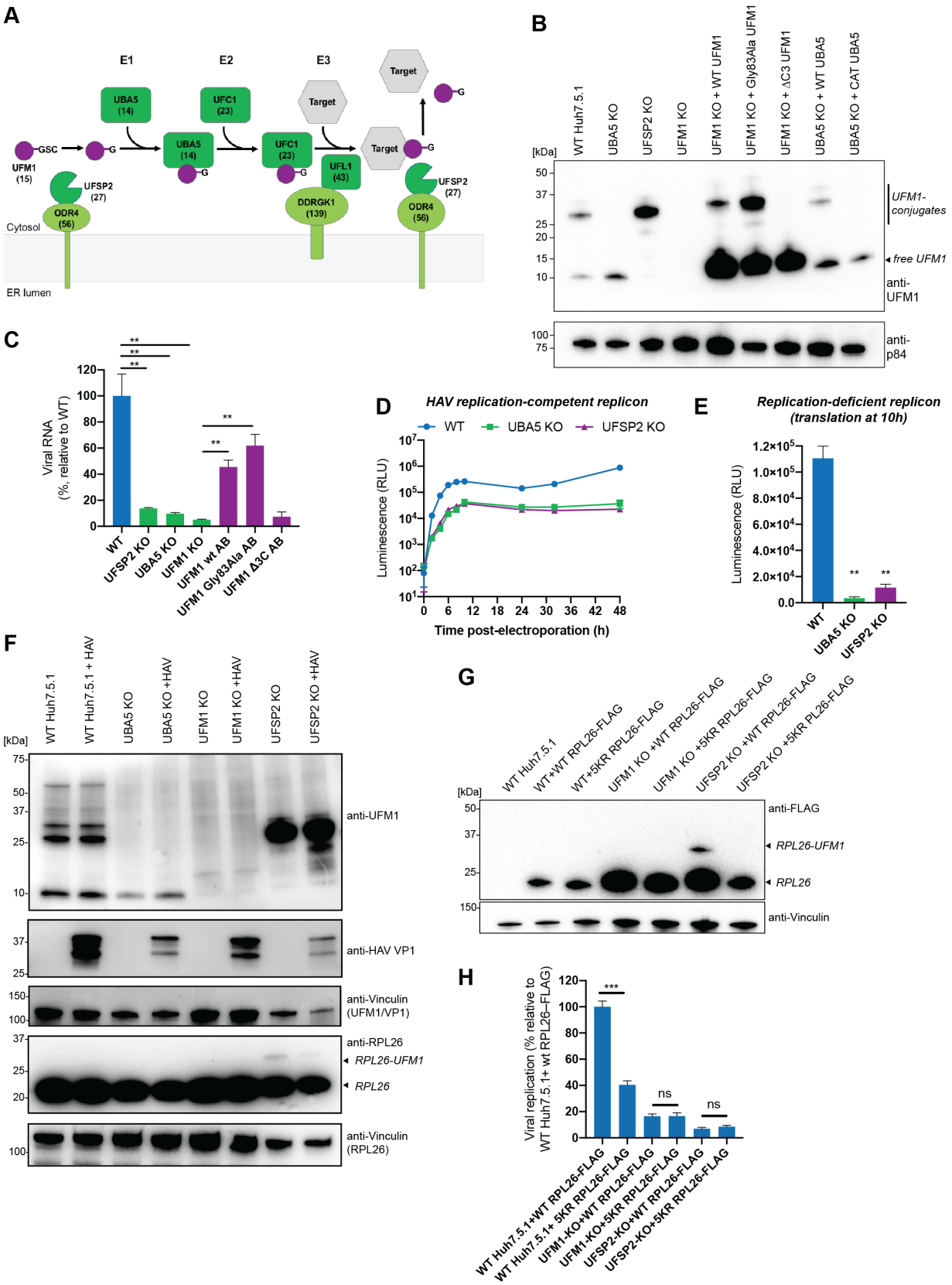
A
E1
E2
E3
UBA5 (14)
UFC1 (23)
Target
GSC
UFM1 (15)
UFSP2 (27)
ODR4 (56)
UFL1 (43)
DDRGK1 (139)
Cytosol
ER lumen
B
WT Huh7.5.1
UBA5 KO
UFSP2 KO
UFM1 KO
UFM1 KO + WT UFM1
UFM1 KO + Gly83Ala UFM1
UFM1 KO + ΔC3 UFM1
UBA5 KO + WT UBA5
UBA5 KO + CAT UBA5
[kDa]
UFM1-conjugates
free UFM1
anti-UFM1
anti-p84
C
Viral RNA (%, relative to WT)
WT
UFSP2 KO
UBA5 KO
UFM1 KO
UFM1 wt AB
UFM1 Gly83Ala AB
UFM1 Δ3C AB
D
HAV replication-competent replicon
WT
UBA5 KO
UFSP2 KO
Luminescence (RLU)
Time post-electroporation (h)
E
Replication-deficient replicon (translation at 10h)
Luminescence (RLU)
WT
UBA5 KO
UFSP2 KO
F
WT Huh7.5.1
WT Huh7.5.1 + HAV
UBA5 KO
UBA5 KO +HAV
UFM1 KO
UFM1 KO +HAV
UFSP2 KO
UFSP2 KO +HAV
[kDa]
anti-UFM1
anti-HAV VP1
anti-Vinculin (UFM1/VP1)
anti-RPL26
RPL26-UFM1
RPL26
anti-Vinculin (RPL26)
G
WT Huh7.5.1
WT+WT RPL26-FLAG
WT+5KR RPL26-FLAG
UFM1 KO +WT RPL26-FLAG
UFM1 KO +5KR RPL26-FLAG
UFSP2 KO +WT RPL26-FLAG
UFSP2 KO +5KR PL26-FLAG
[kDa]
anti-FLAG
RPL26-UFM1
RPL26
anti-Vinculin
H
Viral replication (% relative to WT Huh7.5.1+ wt RPL26–FLAG)
ns
ns
WT Huh7.5.1+WT RPL26-FLAG
WT Huh7.5.1+ 5KR RPL26-FLAG
UFM1-KO+WT RPL26-FLAG
UFM1-KO+5KR RPL26-FLAG
UFSP2-KO+WT RPL26-FLAG
UFSP2-KO+5KR RPL26-FLAG

411 **Figure 3. HAV depends on functional UFM1 conjugation of the ribosomal protein RPL26 for**
412 **optimal translation. (A)** Schematic of cellular UFMylation pathway. (#) indicates rank in gene
413 enrichment analysis of CRISPR screen. **(B)** UFM1 immunoblot of WT, *UFSP2* KO, *UBA5* KO, *UFM1*
414 KO and *UFM1* KO cells complemented with WT, Gly83Ala or ΔC3 UFM1 as well as *UBA5* KO cells
415 complemented with WT or catalytically inactive UBA5. Upper bands represent UFM1 conjugation
416 products and bottom band represents free UFM1. P84 was used as loading control. **(C)**
417 Quantification of HAV RNA in WT, *UFSP2* KO, *UBA5* KO, *UFM1* KO and *UFM1* KO cells
418 complemented with WT, Gly83Ala or ΔC3 UFM1. Viral RNA was normalized to 18S RNA and
419 results are displayed relative to infection in WT cells. **(D)** Timecourse of luciferase activity
420 expressed by electroporated HAV-FLuc subgenomic replicon RNA in WT, *UBA5* KO and *UFSP2* KO
421 cells. **(E)** Luciferase activity from electroporated HAV-FLuc replication-incompetent replicon RNA
422 in WT, *UBA5* KO and *UFSP2* KO cells at 10h post-electroporation. **(F)** Immunoblots of uninfected
423 and HAV infected WT, *UBA5* KO, *UFM1* KO and *UFSP2* KO cells. Membranes were stained with
424 anti-UFM1, anti-HAV VP1 or anti-RPL26 antibodies. Anti-Vinculin served as loading control. **(G)**
425 FLAG immunoblot of WT, *UFM1* KO and *UFSP2* KO cells transduced with lentivirus expressing
426 FLAG-tagged WT RPL26 or 5KR RPL26. Vinculin served as loading control. **(H)** Quantification of
427 HAV RNA in WT, *UFM1* KO and *UFSP2* KO cells expressing WT RPL26 or 5KR RPL26. Viral RNA was
428 normalized to 18S RNA and results are displayed relative to infection in WT cells expressing WT
429 RPL26.
430 For all RT-qPCR experiments, datasets represent means ± s.e.m. (n=3 biological replicates). For
431 luciferase experiments, datasets represent means ± s.d. (n=2 biological replicates) for each

432 timepoint. P values were determined by unpaired two-sided t-tests using GraphPad Prism 8. ns,

433 non-significant; *, $p<0.05$; **, $p<0.01$; ***, $p<0.001$; ****<0.0001.

Figure S5

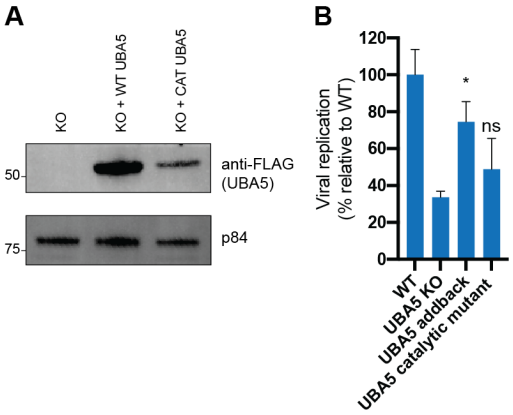

434

435 **Figure S5. HAV depends on catalytically active UBA5, Related to Figure 3. (A)** FLAG immunoblot

436 of lysates from *UBA5* KO cells transduced with FLAG-tagged WT or catalytically inactive (CAT)

437 UBA5. P84 was used as loading control. **(B)** Quantification of HAV RNA in WT, *UBA5* KO and *UBA5*

438 KO complemented with WT or CAT UBA5 3 dpi by RT-qPCR. Viral RNA was normalized to 18S RNA

439 and results are displayed relative to infection in WT cells. Datasets represent means ± s.e.m. (n=3

440 biological replicates). P values were determined by unpaired two-sided t-tests using GraphPad

441 Prism 8. ns, non-significant; *, $p<0.05$.

442

Figure S6

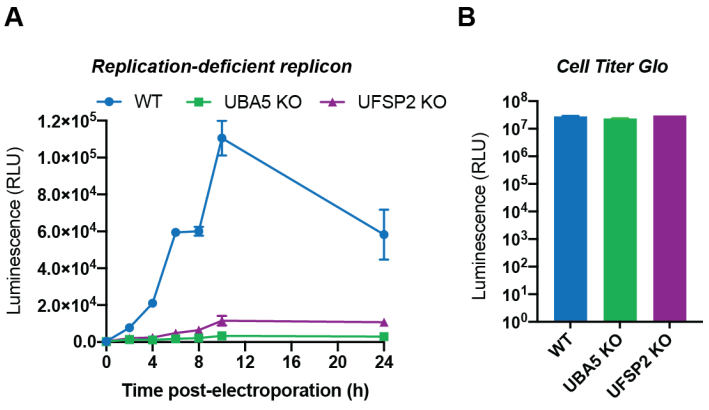

443

444 **Figure S6. HAV translation is impaired in UFMylation deficient cells, Related to Figure 3. (A)**

445 Timecourse of luciferase activity expressed by electroporated HAV-FLuc replication-incompetent

446 replicon RNA in WT, *UBA5* KO and *UFSP2* KO cells. Datasets represent means ± s.d. (n=2 biological

447 replicates) for each timepoint. **(B)** Cell Titer Glo assay to measure cell viability of electroporated

448 WT, *UBA5* KO and *UFSP2* KO cells 24h post-electroporation. Datasets represent means ± s.d. (n=2

449 biological replicates).

450

Figure S7

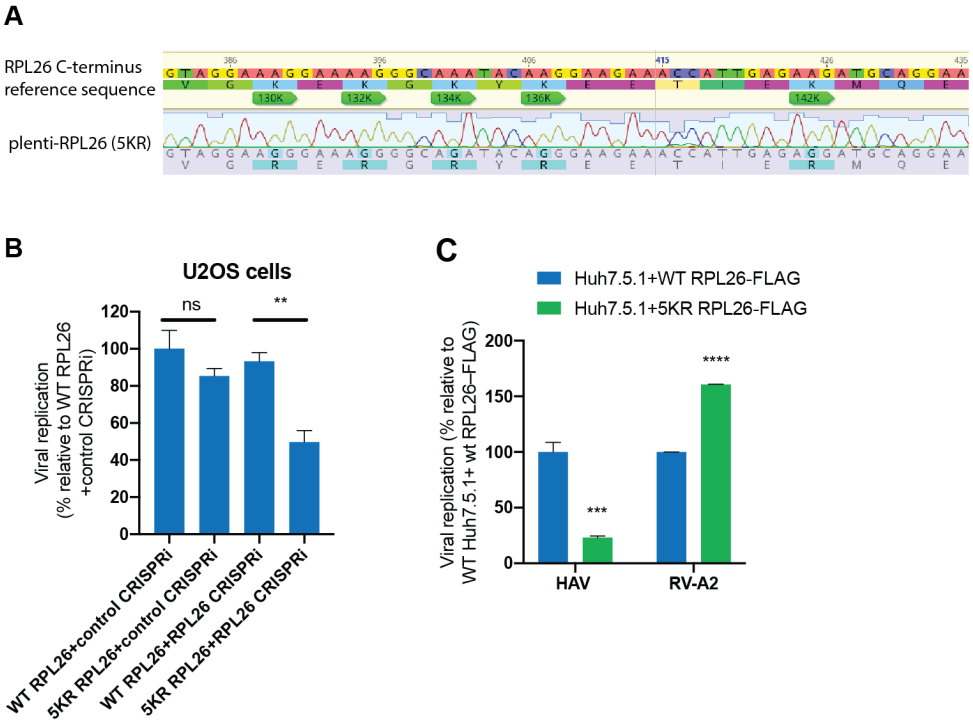

Figure S7. UFM1 conjugation to C-terminal lysines of RPL26 is required for optimal HAV infection, Related to Figure 3. (A) Reference and Sanger sequence of lentiviral construct expressing RPL26 with five lysine to arginine point mutations at C-terminus (5KR). **(B)** Quantification of HAV RNA in U2OS dCas9-KRAB cells expressing WT RPL26 or 5KR RPL26 as well as a control (non-targeting) or RPL26 targeting gRNA. Viral RNA was normalized to 18S RNA and results are displayed relative to infection in cells expressing WT RPL26 and the control gRNA. **(C)** Quantification of HAV and RV-A2 RNA in WT cells transduced with lentivirus expressing FLAG-tagged WT RPL26 or 5KR RPL26. Viral RNA was normalized to 18S RNA and results are displayed relative to infection in WT cells expressing WT RPL26. Dataset represents means ± s.e.m. (n=3 biological replicates). P values were determined by unpaired two-sided t-tests using GraphPad Prism 8. ns, non-significant; *, p<0.05; **, p<0.01; ***, p<0.001; ****<0.0001.

Figure 4

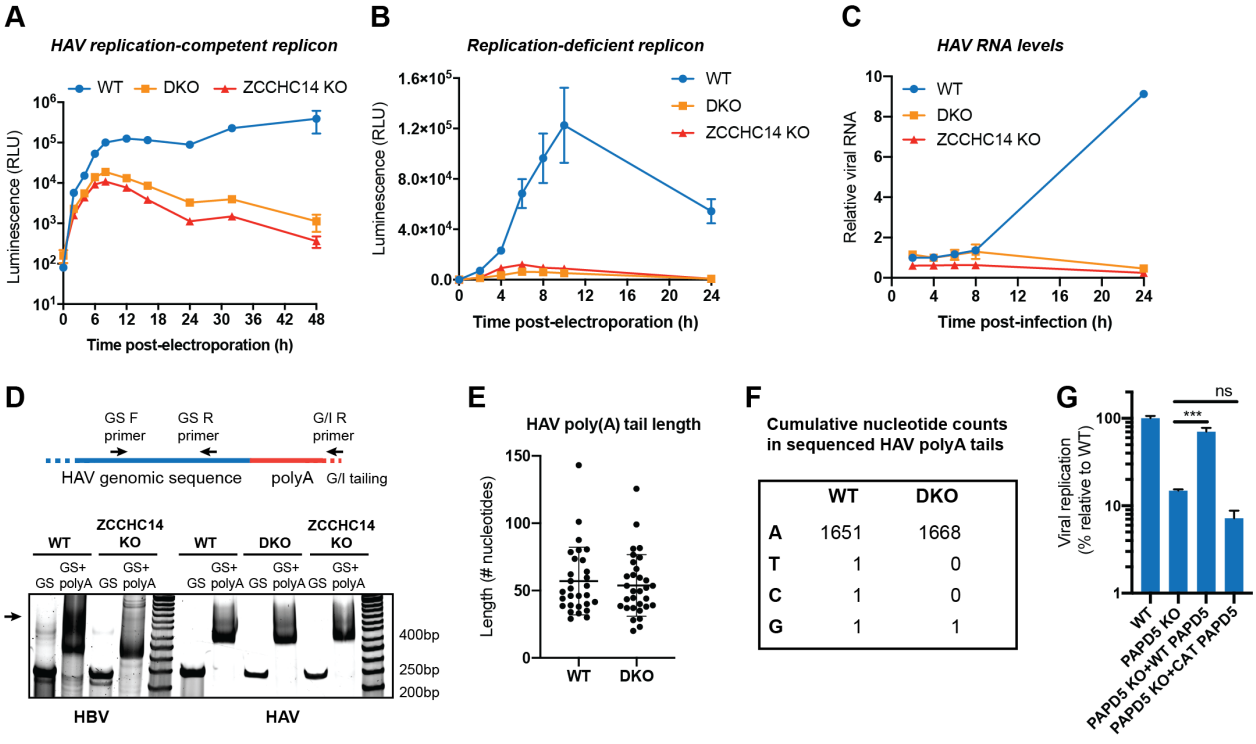

	WT	DKO
A	1651	1668
T	1	0
C	1	0
G	1	1

Figure 4. Catalytic activity of TRAMP-like complexes is important for HAV translation, independent of regulating viral poly(A) tail length or RNA stability. (A) Timecourse of luciferase activity expressed by electroporated HAV-FLuc subgenomic replicon RNA in WT, DKO and *ZCCHC14* KO cells. Datasets represent means ± s.d. (n=2 biological replicates) for each timepoint. **(B)** Timecourse of luciferase activity expressed by electroporated HAV-FLuc replication-incompetent replicon RNA in WT, DKO cells and *ZCCHC14* KO. Datasets represent means ± s.d. (n=2 biological replicates) for each timepoint. **(C)** Quantification of HAV RNA in WT, DKO and *ZCCHC14* KO cells by RT-qPCR. Cells were infected on ice, incubated at 37C for 1h, washed 3 times and harvested at indicated times. Viral RNA was normalized to 18S RNA. Datasets represent means ± s.e.m. (n=3 biological replicates). **(D)** Poly(A) tail length assay. Total RNA from infected WT or KO cells was G/I tailed at 3'ends, reverse transcribed and PCR amplified by either genome-specific (GS) forward and GS reverse primers, or GS forward and G/I reverse primer. PCR products

476 were analyzed by polyacrylamide gel electrophoresis. For HBV, total RNA was collected from
477 infected WT or *ZCCHC14* KO HepG2-NTCP cells 14dpi. For HAV, total RNA was harvested from
478 infected WT, DKO or *ZCCHC14* KO Huh7.5.1 cells 3dpi. Arrow indicates a longer HBV poly(A) tail
479 in WT cells. **(E)** Length distribution of sequenced HAV poly(A) tails. An RNA linker was ligated to
480 3'ends of rRNA-depleted RNA from infected WT or DKO cells followed by reverse transcription
481 and PCR amplification of the HAV poly(A) tail region. PCR products were TOPO cloned and Sanger
482 sequenced. **(F)** Analysis of nucleotide composition of sequenced HAV poly(A) tails from (E). **(G)**
483 Quantification of HAV RNA in WT, *PAPD5* KO and *PAPD5* KO cells complemented with either WT
484 or catalytically inactive (CAT) PAPD5 3 dpi by RT-qPCR. Viral RNA was normalized to 18S RNA and
485 results are displayed relative to infection in WT cells. Datasets represent means ± s.e.m. (n=3
486 biological replicates).
487

Figure S8

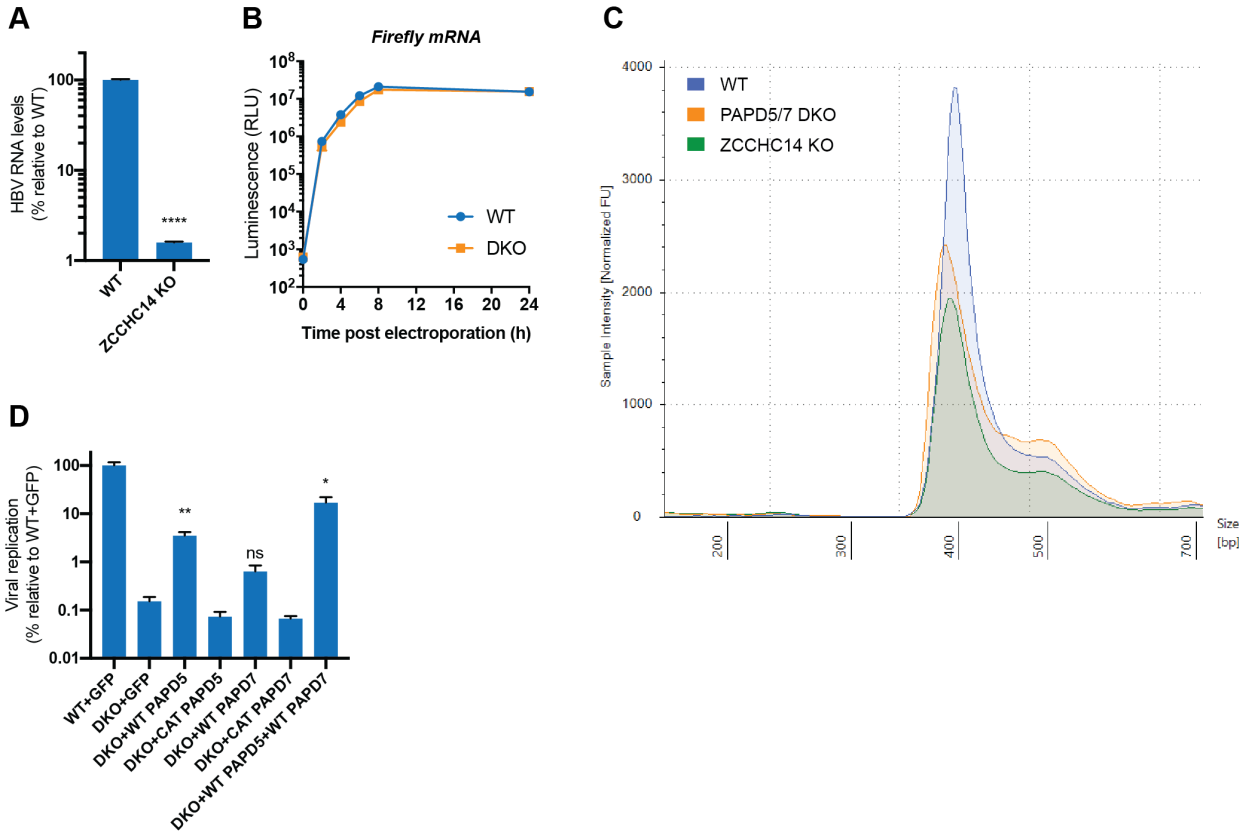

Figure S8. Catalytic activity of TRAMP-like complexes is important for HAV translation, independent of regulating viral poly(A) tail length or RNA stability, Related to Figure 4. (A) Quantification of HBV RNA in WT and *ZCCHC14* KO HepG2-NTCP cells 14dpi. Viral RNA was normalized to 18S RNA and results are displayed relative to infection in WT cells. **(B)** Timecourse of luciferase activity expressed by electroporated firefly mRNA in WT and DKO cells. Datasets represent the means ± s.d. (n=2 biological replicates). **(C)** Electrophoretic analysis of poly(A) tail region of HAV from infected WT, DKO and *ZCCHC14* KO cells at 72hpi. Total RNA was G/I tailed at 3'ends, reverse transcribed and PCR amplified by forward primer ~300bp upstream of HAV poly(A) start site and G/I specific reverse primer. PCR products were analyzed using TapeStation. **(D)** Quantification of HAV RNA in DKO cells transfected with GFP cDNA, PAPD5 WT or CAT cDNA,

499 PAPD7 WT or CAT cDNA, or co-transfected with both PAPD5 and PAPD7 WT cDNAs. Viral RNA
500 was normalized to 18S RNA and results are displayed relative to infection in WT cells transfected
501 with GFP cDNA.
502 For RT-qPCR, datasets represent means ± s.e.m. (n=3 biological replicates). P values were
503 determined by unpaired two-sided t-tests using GraphPad Prism 8. ns, non-significant; *, $p<0.05$;
504 **, $p<0.01$; ****, $p<0.0001$.
505

Figure 5

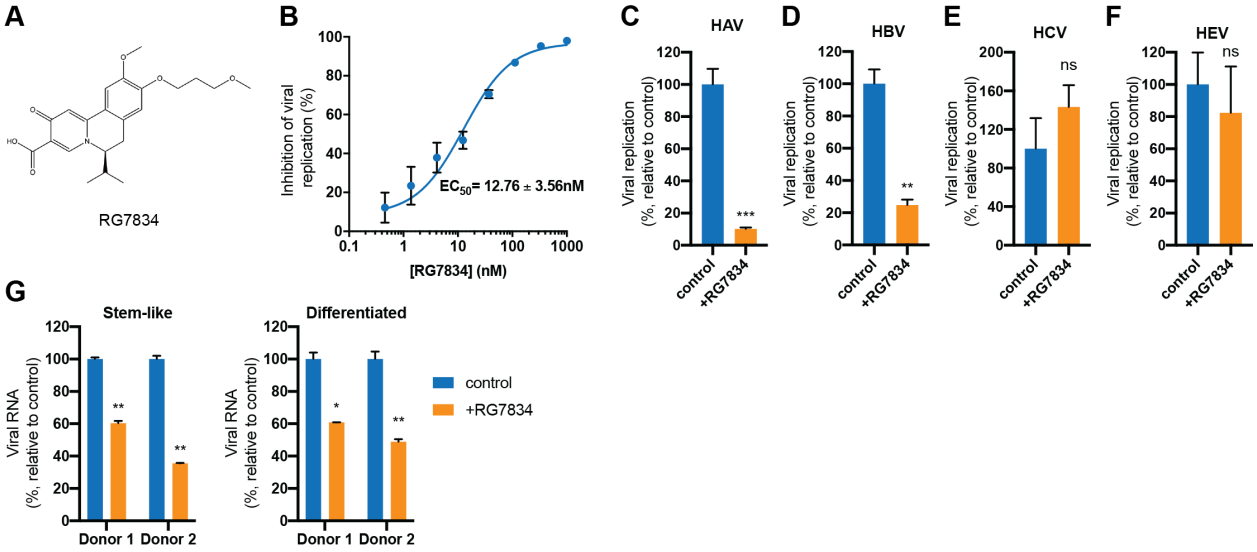

Figure 5. Small molecule inhibition of PAPD5 and PAPD7 reduces HAV infection in human hepatocyte cells and human liver organoids. (A) Chemical structure of RG7834. **(B)** Dose-response curve of HAV RNA levels in Huh7.5.1 cells treated with different RG7834 concentrations as measured by RT-qPCR 3 days post-infection/treatment. Non-linear curve was fitted with least squares regression using GraphPad Prism 8 and EC_{50} was determined. **(C)** Quantification of HAV RNA in control and RG7834 (100 nM) treated Huh7.5.1 cells 3 dpi by RT-qPCR. **(D)** Quantification of HBV total RNA in control and RG7834 (100 nM) treated HepG2-NTCP cells 15 dpi by RT-qPCR. Drug was replenished every 3-4 days. **(E)** Quantification of HCV RNA in control and RG7834 (100 nM) treated Huh7.5.1 cells 3 dpi by RT-qPCR. **(F)** Quantification of HEV RNA in control and RG7834 (100 nM) treated Huh7.5.1 cells by RT-qPCR 6 days post-transfection of viral RNA. **(G)** Quantification of HAV RNA in control and RG7834 (100 nM) treated human liver organoids 7 dpi by RT-qPCR. Organoids were either stem-like or differentiated to adult hepatocytes prior to infection.

520 For all RT-qPCR experiments, viral RNA was normalized to 18S RNA and results are displayed
521 relative to infection in control (DMSO) condition. Datasets in (**B-F**) represent means ± s.e.m. (n=3
522 biological replicates). For organoid experiments (**G**) donor 1 and 2 represent 2 independent
523 biological replicates and qPCR was performed with 2 technical replicates. P values were
524 determined by unpaired two-sided t-tests using GraphPad Prism 8. ns, non-significant; *, $p<0.05$;
525 **, $p<0.01$; ***, $p<0.001$.

Figure S9

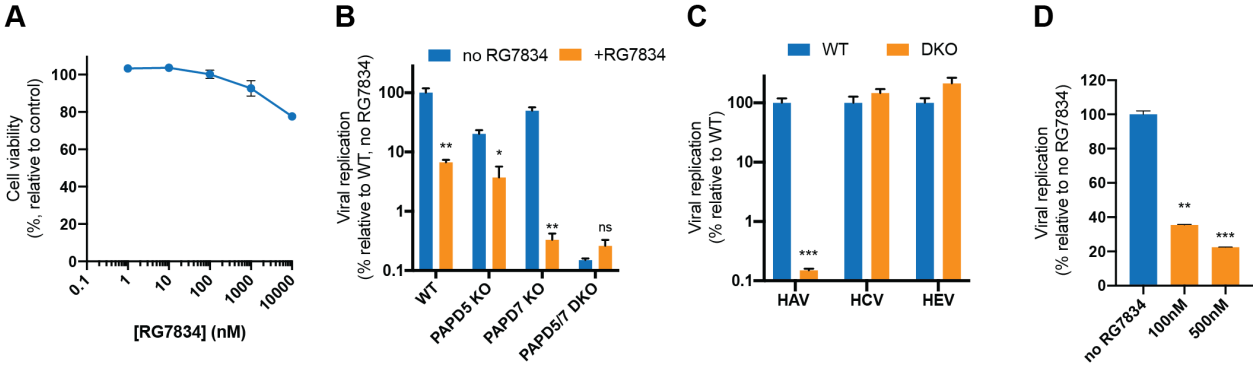

Figure S9. Small molecule inhibition of PAPD5 and PAPD7 reduces HAV infection in human hepatocyte cells and human liver organoids, Related to Figure 5. (A) Cell viability assay of Huh7.5.1 cells treated with different concentrations of RG7834 for 3 days. Dataset represents means ± s.d. (n=3 biological replicates) for each time point and values are relative to DMSO treated control. **(B)** Quantification of HAV RNA in WT, *PAPD5* KO, *PAPD7* KO or DKO cells untreated or treated with 100 nM RG7834 3 dpi by RT-qPCR. **(C)** Quantification of HAV and HCV RNA 3 dpi, and of HEV RNA 5 days post viral RNA transfection in WT or DKO cells using RT-qPCR. **(D)** Quantification of HAV RNA in human liver organoids treated with no, 100 nM or 500 nM RG7834 by RT-qPCR.

For RT-qPCR experiments, viral RNA was normalized to 18S RNA and results are displayed relative to infection in (untreated) WT cells. Datasets represent means ± s.e.m. (n=3 biological replicates). P values were determined by unpaired two-sided t-tests using GraphPad Prism 8. ns, non-significant; *, $p<0.05$; **, $p<0.01$; ***, $p<0.001$; ****<0.0001.

541 **Methods**

542 Cell lines, viruses and reagents

543 Huh7.5.1 (gift from Frank Chisari), HEK293FT (Thermo Scientific) and U2OS cells (gift from Ron
544 Kopito) were cultured in DMEM (Gibco) supplemented with 10% fetal bovine serum (FBS, Omega
545 Scientific), penicillin/streptomycin (Gibco), non-essential amino acids (Gibco) and L-glutamine
546 (Gibco) at 37C and 5% CO_2. HepG2-NTCP-K7 cells (Ko et al., 2018) (gift from Ulrike Protzer) and
547 HepAD38 cells (Ladner et al., 1997) (gift from Christoph Seeger) were cultured in DMEM/F12
548 (Gibco) supplemented with 10% FBS, penicillin/streptomycin, non-essential amino acids, L-
549 glutamine and sodium pyruvate (Gibco) at 37C and 5% CO_2. Cell lines were tested negative for
550 mycoplasma and were authenticated by STR profiling. Hepatitis A virus HM175/18f (NR-137) was
551 obtained through BEI Resources (NIAID, NIH) and propagated in Huh7.5.1 cells grown in adeno
552 expression media (Gibco) supplemented with penicillin/streptomycin, non-essential amino acids
553 and L-glutamine. Supernatant was collected 5-12 dpi and filtered (0.45 micron). To generate
554 concentrated HAV stocks, supernatant was incubated with 8% PEG-8000 at 4C overnight,
555 centrifuged at 3,200g for 60min and pellet was resuspended in a small volume of DMEM with
556 10% FBS and aliquoted. For the generation of HAV-Nluc (gift from Stanley Lemon) (Rivera-Serrano
557 et al., 2019), the infectious clone plasmid was linearized, RNA was *in-vitro* transcribed using
558 MEGAscript T7 Transcription Kit (Invitrogen) and transfected into Huh7.5.1 cells using TransIT-
559 LT1 Transfection Reagent (Mirus Bio). Subsequently, cell supernatant was collected 8-13dpi,
560 filtered and aliquoted. Purified encephalomyocarditis virus (NR-46441) was obtained through BEI
561 Resources (NIAID, NIH). Enterovirus 71 (MP4), rhinovirus A2 and HCV JFH1 stocks were kindly
562 provided by Jan Carette. For HBV production, supernatant was collected from HepAD38 cells,

563 filtered (0.45 micron), and concentrated using 8% PEG-8000 as described above. The HEV
564 infectious clone (genotype 3) was obtained from the NIH/NIAID and viral RNA was generated by
565 *in-vitro* transcription from linearized plasmid (Shukla et al., 2012). For virus stocks, titers were
566 determined by plaque- or focus-forming assay. RG7834 was purchased from MedKoo Biosciences
567 and resuspended in DMSO at 50mg/ml. Puromycin and blasticidin were obtained from Gibco.
568
569 CRISPR host factor screen
570 Huh7.5.1 cells were stably transduced with lentivirus from lentiCas9-Blast (Addgene #52962, gift
571 from Feng Zhang) and subsequently selected using blasticidin. Next, a total of 300 million
572 Huh7.5.1-Cas9 cells were then separately transduced with the lentiviral gRNA sublibraries A and
573 B of the human GeCKO v2 library (Addgene #1000000049, gift from Feng Zhang) at a multiplicity
574 of infection (MOI) of 0.3. Each sublibrary contained 3 guides per gene. Subsequently, the cells
575 were selected using puromycin and expanded for 10 days. A total of 60 million mutagenized cells
576 for each sublibrary (A and B) were collected for genomic DNA extraction, and a total of 45 million
577 mutagenized cells for each sublibrary were infected with 15ml of unconcentrated HAV
578 HM175/18f per T175 flask (1:1 diluted with fresh DMEM media). An additional 15ml of media
579 was added after 2h. Media was refreshed 4 and 8dpi and surviving cells were collected 12dpi for
580 genomic DNA extraction using QIAamp DNA Blood Maxi Kit (Qiagen). gRNA encoding DNA
581 sequences were amplified in a two-step nested PCR using KAPA HiFi HotStart ReadyMixPCR Kit
582 (Kapa Biosystems) and sequenced on an Illumina NextSeq (High Output) (for primer sequences,
583 see Table S3). For analysis, reads were aligned to gRNA reference table and enrichment of each
584 gRNA was calculated by comparing the relative abundance in the selected and unselected cell

585 population. Gene enrichment analysis was performed using the RIGER weighted sum algorithm
586 as well as MaGeCK analysis (Li et al., 2014; Luo et al., 2008). Gene ontology analysis of enriched
587 genes in target list (containing 72 genes with RIGER p-value < 0.001) was performed using GOrilla
588 (Eden et al., 2009). For comparison with other CRISPR host factor screens, RIGER-based gene
589 enrichment analysis was used for HCV and HBV screens, and MaGeCK-based analysis for EV-D68
590 and HRV-C15 screens.
591
592 Generation of clonal KO cell lines
593 Oligos containing gRNA sequence were annealed and ligated into pX458 (Addgene #48138, gift
594 from Feng Zhang). Cells were transfected with pX458 constructs using Lipofectamine 3000
595 (Invitrogen) and two days later GFP positive cells were single-cell sorted into 96-well plates using
596 a Sony SH800 cell sorter. For genotyping, genomic DNA was isolated from obtained clones using
597 QuickExtract (Lucigen), the gRNA-targeted sites PCR amplified and the products Sanger-
598 sequenced. Obtained sequences were compared to reference sequences for indel mutations or
599 large deletion. A list of all used gRNA oligo and genotyping primer sequences can be found in
600 Table S3.
601
602 Intracellular RNA RT-qPCR assays
603 Cells were plated in 96-well plates (in triplicates for each condition) and infected the next day
604 with virus at the following MOIs: HAV (~5-10 FFU/cell), RV-A2 (~1 PFU/cell), EV-71 (~0.2 PFU/cell),
605 EMCV (~0.2 PFU/cell), HCV (~1 FFU/cell) and HBV (~1 FFU/cell). Cells were harvested, lysates
606 reverse transcribed and quantitative PCR performed on a Bio-Rad CFX96 Touch system using the

607 Power SYBR Cells-to-CT kit (Invitrogen). All viral RNA levels were normalized to 18S levels. Primer
608 sequences can be found in Table S3.
609
610 Quantification of extracellular viral RNA
611 Cells were plated in 96-well plates (duplicates for each condition) and infected with HAV at an
612 MOI of 5. After 4h, inoculum was removed and cells were washed with PBS. At 3 dpi 100µl of
613 supernatant was collected and RNA was isolated using the Qiagen Viral RNA Mini kit. Eluted RNA
614 was reversed transcribed and analyzed by qPCR as described above. For determination of
615 genome copies in-vitro transcribed HAV RNA was serially diluted and also quantified by RT-qPCR.
616
617 Viral attachment and entry assay
618 96-well plates containing WT, *SLC35A1* KO or *HAVCR1* KO Huh7.5.1 cells were chilled on ice
619 before infection with HAV HM175/18f at an MOI of 500 FFU/cell. Cells were incubated for 1h on
620 ice before moving them to a 37C incubator. At each harvest timepoint, cells were washed three
621 times with PBS and processed for RT-qPCR as described above.
622
623 HAV nanoluciferase reporter assay
624 Cells were plated in 96-well plates and infected the next day with equal amounts of HAV-Nluc.
625 Lysates were harvested by washing once with PBS wash followed by addition of 22µl of Passive
626 Lysis Buffer (Promega) under shaking for 15min. For luminescence readout, 15µl of lysate were
627 mixed with 50µl of Nano-Glo assay buffer (Promega) in a flat bottom white-walled luminescence

628 plate, incubated for 5min at room temperature and read on an EnVision plate reader
629 (PerkinElmer).
630
631 Complementation of KO cells with cDNA
632 UBA5 cDNA was obtained from Dharmacon (DNA Accession: BC009737, Clone ID: 3879061). To
633 generate cDNA encoding catalytically inactive enzyme, a Cys250Arg mutation was introduced by
634 PCR. Additionally, a C-terminal FLAG-tag was added to WT and CAT cDNA sequences. UFM1 was
635 obtained from Dharmacon (cDNA Accession: BC005193, Clone ID: 3829206). N-terminal FLAG and
636 C-terminal mutations (Gly83Ala or ΔC3 (deletion of GlySerCys)) were introduced by PCR. For
637 RPL26, cDNA was obtained from OriGene (RC209922) and a C-terminal FLAG-tag was added. To
638 introduce 5KR mutations, a reverse primer containing point 5 mutations was used. ZCCHC14
639 cDNA was obtained from Dharmacon (cDNA Accession: BC101478, Clone ID: 8068984). The N-
640 terminus was extended using a Gblock (Integrated DNA Technologies) resembling the protein
641 coding sequence for a longer isoform (1086 amino acids, ENST00000671377.1) to match the
642 molecular weight of ZCCHC14 detected in WT Huh7.5.1 by immunoblot. PCR products were gel-
643 purified and cloned into EcoRV-cut pLenti CMV Puro DEST (w118-1) (Addgene #17452, gift from
644 Eric Campeau & Paul Kaufman) using NEBuilder HiFi DNA Assembly Master Mix (New England
645 BioLabs). Lentivirus was produced in HEK293FT and collected 48h post-transfection. KO cells
646 were transduced with filtered, lentiviral containing supernatant under addition of polybrene and
647 selected using 4 µg/ml puromycin for 3-4 days. For PAPD5 and PAPD7, pCI3 plasmids with WT or
648 catalytic mutant cDNA sequences were kindly provided by V. Narry Kim and were described
649 previously (Lim et al., 2018). For transient complementation, plasmids were transfected into WT

650 or DKO cells using TransIT-LT1 Transfection Reagent (Mirus Bio), and transfected cells were
651 plated in 96-wells the next day for HAV infection. To generate stable cell lines, cDNA sequences
652 were cloned into the PB-CMV-MCS-EF1α-Puro vector (PB510B-1, SBI System Biosciences) where
653 the CMV promoter was replaced by a PGK promoter. Plasmids were co-transfected together with
654 a plasmid expressing piggyBac transposase into *PAPD5* KO cells, which were subsequently
655 selected with puromycin for 5 days starting 3 days post-transfection. All primer sequences can
656 be found in Table S3.
657
658 Immunoblotting
659 Cell were lysed using Laemmli SDS sample buffer containing 5% beta-mercaptoethanol and boiled
660 for 10min. Lysates were separated by SDS-PAGE on pre-cast Bio-Rad 4-15% poly-acrylamide gels
661 in Bio-Rad Mini-Protean electrophoresis system. Proteins were transferred onto PVDF
662 membranes using Bio-Rad Trans-Blot Turbo transfer system. PVDF membranes were blocked
663 with PBS buffer containing 0.1% Tween-20 and 5% non-fat milk. Blocked membranes were
664 incubated with primary antibody diluted in blocking buffer and incubated overnight at 4C on a
665 shaker. Primary antibodies were detected by incubating membranes with 1:4000 dilution of HRP-
666 conjugated (Southern Biotech) or 1:5000 dilution of IRDye-conjugated (LI-COR) secondary anti-
667 mouse and anti-rabbit antibodies for 1 h at room temperature. Blots were visualized using a
668 ChemiDoc MP Imaging System (Bio-Rad). The following primary antibodies (and their dilutions)
669 were used in this study: p84 (Genetex, GTX70220) at 1:1000, GAPDH (SCBT, sc-32233) at 1:1000,
670 vinculin (SCBT, sc-73614), 1:1000, eIF4B (SCBT, sc-376062) at 1:250, VPS4A (SCBT, sc-393428) at
671 1:300, SLC35A1 (Proteintech, 16342-1-AP) at 1:250, HAV VP1 (LS Bio, LS-C137674-100) at 1:1000,

672 FLAG M2 (Sigma, F1804) at 1:1000, UFM1 (Abcam, ab109305) at 1:1000, UBA5 (Bethyl, A304-
673 115A) at 1:2500, UFSP2 (SCBT, sc-376084) at 1:100, RPL26 (Bethyl, A300-686A) at 1:1000, PAPD5
674 (Atlas Antibodies, HPA042968) at 1:1000 and ZCCHC14 (Bethyl, A303-096A) at 1:1000. For
675 SLC35A1, lysates from 10^6 cells were immunoprecipitated using 4 µg anti-SLC35A1 antibody and
676 Protein G magnetic Dynabeads (Thermo Scientific, 10-003-D) overnight at 4C prior to
677 immunoblotting to enhance signal and specificity of signal.
678
679 Replicon assay
680 The replicon plasmids pLuc-HAV/18f and pLuc-HAV/18f-$3D^{pol}$GDD→GAA (replication-defective
681 mutant) were kindly provided by Stanley Lemon and were described previously (González-López
682 et al., 2018). Plasmids were linearized using MluI-HF (New England BioLabs), RNA was generated
683 using the MEGAscript T7 Kit (Invitrogen) and subsequently purified by lithium chloride
684 precipitation. For electroporation, 1-2 million cells were washed three times in PBS, resuspended
685 in 100µl SF Nucleofector solution (Lonza), mixed with 250ng replicon RNA per 80k cells,
686 transferred to a 100 µl nucleocuvette and pulsed using the program FF-137 on an Amaxa 4D-
687 Nucleofector X Unit (Lonza). Cells were then resuspended in equilibrated, antibiotic-free
688 medium, distributed into 96-wells and lysed at different timepoints post-electroporation using
689 40µl Passive Lysis buffer (Promega). Luminescence was measured using Luciferase Assay System
690 (Promega) on a white-walled luminescence plate with an EnVision plate reader (PerkinElmer).
691
692 Poly(A) tail length assay by polyacrylamide gel electrophoresis

693 Cells were infected with HAV HM175/18f (MOI=10) and harvested 3 days post-infection using
694 Trizol (Invitrogen). RNA was purified with Direct-zol RNA Microprep columns (Zymo Research).
695 HAV poly(A) tails were analyzed using the Poly(A) Tail-Length Assay Kit (Thermo Scientific)
696 according to the manufacturer's instructions. Briefly, 1µg total RNA per condition was used as
697 input for G/I tailing reaction followed by reverse transcription. Next, RT products were amplified
698 using either the genome-specific (GS) forward and GS reverse primer, or GS forward and G/I
699 specific reverse primer. PCR products were analyzed using polyacrylamide gel electrophoresis on
700 a 5% Mini-PROTEAN Tris/Boric Acid/EDTA (TBE) gel in TBE buffer (100V for 60min). Gel was
701 stained with SYBR Gold (diluted 1:10000 in TBE buffer) for ~30min in the dark and imaged on a
702 ChemiDoc MP Imaging System (Bio-Rad).
703
704 Poly(A) tail sequencing
705 RNA was isolated from infected cells as described above. Ribosomal RNA (rRNA) was depleted
706 from 1µg total RNA by addition of rRNA Removal Mix – Gold (Illumina) followed by incubation at
707 68C for 5min, addition of rRNA Removal Beads (Illumina), removal of supernatant while tubes
708 are on a magnetic rack, and finally elution of rRNA-depleted RNA. Next, a 5´ adenylated, 3´
709 blocked oligodeoxynucleotide RNA linker (S1315S, New England BioLabs) was ligated to the 3'
710 ends of RNAs by incubation with RNA ligase 2, truncated (New England BioLabs) for 3h at 22C.
711 Ligation products were then reverse transcribed using a primer, which is reverse complement to
712 the RNA linker, and Superscript IV (Invitrogen). Finally, HAV poly(A) tails were specifically
713 amplified in a nested PCR, cloned into the pCRBlunt II-TOPO vector (Invitrogen) and Sanger

714 sequenced (Quintarabio). Number of adenosines downstream of the HAV 3'UTR region and
715 occurrence of non-adenosine nucleotides were counted.
716
717 Tapestation analysis of poly(A) tails of replicon RNA
718 10^6 cells were electroporated with *in-vitro* transcribed replicon RNA containing a 40bp long
719 poly(A) tail as described above. For each timepoint, cells were washed with PBS, trypsinized,
720 pelleted and lysed using Trizol followed by RNA extraction with Direct-zol columns. Total RNA
721 was G/I tailed, reverse transcribed and poly(A) tail region was amplified using the GS forward
722 primer and G/I reverse primer. Products were analyzed using a High Sensitivity D1000
723 ScreenTape System (Agilent).
724
725 Cell viability assay
726 Huh7.5.1 cells were treated with different concentrations of RG7834 for 3 days and viability was
727 measured using Cell Titer Glo (Promega) according to the manufacturer's instructions.
728
729 Culture and HAV infection of human liver organoids
730 Bi-potent stem cell organoids were generated as previously described (Broutier et al., 2016; Huch
731 et al., 2015). Briefly, liver tissue samples from healthy resection margins of partial hepatectomies
732 were obtained through the Ibrahim El-Hefni Liver Biorepository at the California Pacific Medical
733 Center Research Institute. Following tissue digest, the heterogeneous mixture of single cells was
734 suspended in reduced growth factor BME2 (Basement Membrane Extract, Type 2, Trevigen).
735 From this mixture, 50 µL drops containing 1,000 to 20,000 cells were seeded in 24-well

736 suspension culture plates (GreinerBio). Drops were incubated at 37C for >20 min and solidified.
737 After this, 500 µL of expansion media (EM) was added to each well. Expansion media is basal
738 media (Advanced DMEM/F12 with 1% penicillin/streptomycin, 1% Glutamax, and 10 mM HEPES
739 (all from ThermoFisher) supplemented with 1% N2 (Gibco), 1% B27 (Gibco), 1 mM N-
740 Acetylcysteine (Sigma-Aldrich), 10 nM [Leu^{15}]-gastrin I human (Sigma-Aldrich), 10% (vol/vol) R-
741 spondin1 conditioned media (generated as described in (Broutier et al., 2016)), and 10 mM
742 Nicotinamide (Sigma-Aldrich). Expansion media additionally contains 50 ng/ml recombinant
743 human EGF, 25 ng/ml recombinant human HGF, 100 ng/ml recombinant human FGF10, 10 µM
744 Forskolin, and 5 µM A83-01 (all from Stem Cell Technologies). Expansion media was replaced
745 every 3-4 days. Organoids in expansion media grew in culture for 4-6 months and needed to be
746 routinely passaged with TRYPLE (Gibco). To induce differentiation to a hepatocyte-like fate,
747 expansion media was supplemented with 25 ng/ml BMP7 (ProSpec) for 3-4 days. After this, media
748 was changed to differentiation media (DM). Differentiation media is basal media supplemented
749 with 1% N2, 1% B27, 1 mM N-acetylcysteine, 10 nM [Leu^{15}]-gastrin I human, 50 ng/ml EGF, 25
750 ng/ml HGF, 0.5 µM A83-01, 25 ng/ml BMP7, 3 µM dexamethasone (Sigma-Aldrich), 10 µM DAPT
751 (Stem Cell Technologies), and 100 ng/ml recombinant human FGF19 (ProSpec). Differentiation
752 media was changed every 3-4 days for a period of 3-15 days. For HAV infection, organoid lines
753 from two non-viral donors were spin-infected with the HM175/18f strain of HAV as follows.
754 Organoids from EM and DM d3 conditions were collected and lightly dissociated by a 3 min
755 incubation at 37°C with TRYPLE. Cells were then suspended in basal media containing 10 µM Y-
756 27632 (Stem Cell Technologies) and counted. These cells were mixed with HAV at an MOI of 500
757 FFU/cell in the presence and absence of RG7834 at 100 or 500 nM. Cell suspensions were then

758 added to a 24-well suspension culture plate. The plate was centrifuged at 600 x g for 1 h at room
759 temperature, followed by a 2 h incubation at 37C. After this, cells were collected and washed 3x
760 in basal media. Washed cells were seeded in fresh BME2 drops in a new 24-well suspension
761 culture plate. At 7 days post-infection, infected organoid samples were washed 2x in cold basal
762 media, and cell pellets were lysed in Trizol.
763
764 Statistical analysis
765 Prism 8 (GraphPad Software) was used for statistical analysis. Statistical tests and p-value
766 definitions are listed in the figure legends.
767
768 **Supplementary files**
769 Table S1: Gene enrichment analysis of HAV CRISPR screen.
770 Table S2: Gene ontology analysis for hits of HAV CRISPR screen.
771 Table S3: Oligo sequences.
772
773 **Data availability**
774 Raw sequencing data for CRISPR KO screen is deposited at the EMBL-EBI ArrayExpress
775 (https://www.ebi.ac.uk/arrayexpress/) under the accession number E-MTAB-8646.
776
777 **Author contributions**
778 JK and ASP were responsible for design and execution of experiments, data analysis and
779 manuscript preparation. RW performed comparative analysis of CRISPR screens and assisted with

780 molecular biology experiments. NLM conducted organoid experiments under the supervision of
781 MO. ASP conceptualized and supervised the study.
782
783 **Acknowledgments**
784 We would like to thank Don Ganem for helpful discussions and critically reading the manuscript,
785 Sandra Schmid for valuable feedback on the manuscript, the Biohub Genomics platform for help
786 with sequencing, James Webber for assistance with the CRISPR screen analysis, and members of
787 the Biohub Infectious Disease Initiative for helpful discussions. We would like to acknowledge
788 Drs. Stanley Lemon (University of North Carolina, Chapel Hill), Jan Carette (Stanford University),
789 V. Narry Kim (Seoul National University), Ron Kopito (Stanford University), Ulrike Protzer
790 (Technical University Munich), Feng Zhang (Broad Institute), Christoph Seeger (Fox Chase Cancer
791 Center) and Suzanne Emerson (NIH) for providing critical reagents. We also acknowledge Drs.
792 Stewart Cooper and Ann Erickson, who oversee the Ibrahim El-Hefni Liver Biorepository at the
793 California Pacific Medical Center Research Institute and provided patient tissue samples used to
794 generate liver organoids. The research was funded by the Chan Zuckerberg Biohub (ASP) and by
795 NIH/NIDA grants AI097552 and DP1DA038043-01 (MO).
796
797

798 **References**

799 Ali IK, McKendrick L, Morley SJ, Jackson RJ. 2001. Activity of the hepatitis A virus IRES requires
800 association between the cap-binding translation initiation factor (eIF4E) and eIF4G. *J*
801 *Virol* **75**:7854–7863. doi:10.1128/jvi.75.17.7854-7863.2001
802 Avanzino BC, Fuchs G, Fraser CS. 2017. Cellular cap-binding protein, eIF4E, promotes
803 picornavirus genome restructuring and translation. *Proc Natl Acad Sci* **114**:9611–9616.
804 doi:10.1073/pnas.1704390114
805 Baggen J, Thibaut HJ, Staring J, Jae LT, Liu Y, Guo H, Slager JJ, Bruin JW de, Vliet ALW van,
806 Blomen VA, Overduin P, Sheng J, Haan CAM de, Vries E de, Meijer A, Rossmann MG,
807 Brummelkamp TR, Kuppeveld FJM van. 2016. Enterovirus D68 receptor requirements
808 unveiled by haploid genetics. *Proc Natl Acad Sci* **113**:1399–1404.
809 doi:10.1073/pnas.1524498113
810 Bergamini G, Preiss T, Hentze MW. 2000. Picornavirus IRESes and the poly(A) tail jointly
811 promote cap-independent translation in a mammalian cell-free system. *RNA* **6**:1781–
812 1790.
813 Berndt H, Harnisch C, Rammelt C, Stöhr N, Zirkel A, Dohm JC, Himmelbauer H, Tavanez J-P,
814 Hüttelmaier S, Wahle E. 2012. Maturation of mammalian H/ACA box snoRNAs: PAPD5-
815 dependent adenylation and PARN-dependent trimming. *RNA* **18**:958–972.
816 doi:10.1261/rna.032292.112
817 Boele J, Persson H, Shin JW, Ishizu Y, Newie IS, Søkilde R, Hawkins SM, Coarfa C, Ikeda K,
818 Takayama K, Horie-Inoue K, Ando Y, Burroughs AM, Sasaki C, Suzuki C, Sakai M, Aoki S,
819 Ogawa A, Hasegawa A, Lizio M, Kaida K, Teusink B, Carninci P, Suzuki H, Inoue S,
820 Gunaratne PH, Rovira C, Hayashizaki Y, de Hoon MJL. 2014. PAPD5-mediated 3'
821 adenylation and subsequent degradation of miR-21 is disrupted in proliferative disease.
822 *Proc Natl Acad Sci U S A* **111**:11467–11472. doi:10.1073/pnas.1317751111
823 Borman AM, Kean KM. 1997. Intact Eukaryotic Initiation Factor 4G Is Required for Hepatitis A
824 Virus Internal Initiation of Translation. *Virology* **237**:129–136.
825 doi:10.1006/viro.1997.8761
826 Broutier L, Andersson-Rolf A, Hindley CJ, Boj SF, Clevers H, Koo B-K, Huch M. 2016. Culture and
827 establishment of self-renewing human and mouse adult liver and pancreas 3D organoids
828 and their genetic manipulation. *Nat Protoc* **11**:1724–1743. doi:10.1038/nprot.2016.097
829 CDC. 2019. Widespread person-to-person outbreaks of hepatitis A across the United States |
830 CDC. https://www.cdc.gov/hepatitis/outbreaks/2017March-HepatitisA.htm
831 Chen C, Itakura E, Weber KP, Hegde RS, de Bono M. 2014. An ER complex of ODR-4 and ODR-
832 8/Ufm1 specific protease 2 promotes GPCR maturation by a Ufm1-independent
833 mechanism. *PLoS Genet* **10**:e1004082. doi:10.1371/journal.pgen.1004082
834 Das A, Barrientos R, Shiota T, Madigan V, Misumi I, McKnight KL, Sun L, Li Z, Meganck RM, Li Y,
835 Kaluzna E, Asokan A, Whitmire JK, Kapustina M, Zhang Q, Lemon SM. 2020. Gangliosides
836 are essential endosomal receptors for quasi-enveloped and naked hepatitis A virus. *Nat*
837 *Microbiol*. doi:10.1038/s41564-020-0727-8
838 Das A, Hirai-Yuki A, González-López O, Rhein B, Moller-Tank S, Brouillette R, Hensley L, Misumi I,
839 Lovell W, Cullen JM, Whitmire JK, Maury W, Lemon SM. 2017. TIM1 (HAVCR1) Is Not

840 Essential for Cellular Entry of Either Quasi-enveloped or Naked Hepatitis A Virions. *mBio*
841 **8**. doi:10.1128/mBio.00969-17
842 Diep J, Ooi YS, Wilkinson AW, Peters CE, Foy E, Johnson JR, Zengel J, Ding S, Weng K-F, Laufman
843 O, Jang G, Xu J, Young T, Verschueren E, Kobluk KJ, Elias JE, Sarnow P, Greenberg HB,
844 Hüttenhain R, Nagamine CM, Andino R, Krogan NJ, Gozani O, Carette JE. 2019.
845 Enterovirus pathogenesis requires the host methyltransferase SETD3. *Nat Microbiol*.
846 doi:10.1038/s41564-019-0551-1
847 Ding S, Diep J, Feng N, Ren L, Li B, Ooi YS, Wang X, Brulois KF, Yasukawa LL, Li X, Kuo CJ,
848 Solomon DA, Carette JE, Greenberg HB. 2018. STAG2 deficiency induces interferon
849 responses via cGAS-STING pathway and restricts virus infection. *Nat Commun* **9**:1–8.
850 doi:10.1038/s41467-018-03782-z
851 Drake MJ, Brennan B, Jr KB, Bart SM, Sherman E, Szemiel AM, Minutillo M, Bushman FD, Bates
852 P. 2017. A role for glycolipid biosynthesis in severe fever with thrombocytopenia
853 syndrome virus entry. *PLOS Pathog* **13**:e1006316. doi:10.1371/journal.ppat.1006316
854 Eden E, Navon R, Steinfeld I, Lipson D, Yakhini Z. 2009. GOrilla: a tool for discovery and
855 visualization of enriched GO terms in ranked gene lists. *BMC Bioinformatics* **10**:48.
856 doi:10.1186/1471-2105-10-48
857 Feng Z, Hensley L, McKnight KL, Hu F, Madden V, Ping L, Jeong S-H, Walker C, Lanford RE,
858 Lemon SM. 2013. A pathogenic picornavirus acquires an envelope by hijacking cellular
859 membranes. *Nature* **496**:367–371. doi:10.1038/nature12029
860 Gerakis Y, Quintero M, Li H, Hetz C. 2019. The UFMylation System in Proteostasis and Beyond.
861 *Trends Cell Biol* **29**:974–986. doi:10.1016/j.tcb.2019.09.005
862 Go CD, Knight JDR, Rajasekharan A, Rathod B, Hesketh GG, Abe KT, Youn J-Y, Samavarchi-
863 Tehrani P, Zhang H, Zhu LY, Popiel E, Lambert J-P, Coyaud É, Cheung SWT, Rajendran D,
864 Wong CJ, Antonicka H, Pelletier L, Raught B, Palazzo AF, Shoubridge EA, Gingras A-C.
865 2019. A proximity biotinylation map of a human cell. *bioRxiv* 796391.
866 doi:10.1101/796391
867 González-López O, Rivera-Serrano EE, Hu F, Hensley L, McKnight KL, Ren J, Stuart DI, Fry EE,
868 Lemon SM. 2018. Redundant Late Domain Functions of Tandem VP2 YPX3L Motifs in
869 Nonlytic Cellular Egress of Quasi-enveloped Hepatitis A Virus. *J Virol* **92**.
870 doi:10.1128/JVI.01308-18
871 Gosert R, Chang KH, Rijnbrand R, Yi M, Sangar DV, Lemon SM. 2000. Transient expression of
872 cellular polypyrimidine-tract binding protein stimulates cap-independent translation
873 directed by both picornaviral and flaviviral internal ribosome entry sites In vivo. *Mol Cell*
874 *Biol* **20**:1583–1595. doi:10.1128/mcb.20.5.1583-1595.2000
875 Graff J, Cha J, Blyn LB, Ehrenfeld E. 1998. Interaction of poly(rC) binding protein 2 with the 5'
876 noncoding region of hepatitis A virus RNA and its effects on translation. *J Virol* **72**:9668–
877 9675.
878 Hamill S, Wolin SL, Reinisch KM. 2010. Structure and function of the polymerase core of
879 TRAMP, a RNA surveillance complex. *Proc Natl Acad Sci U S A* **107**:15045–15050.
880 doi:10.1073/pnas.1003505107
881 Han J, Perez JT, Chen C, Li Y, Benitez A, Kandasamy M, Lee Y, Andrade J, tenOever B,
882 Manicassamy B. 2018. Genome-wide CRISPR/Cas9 Screen Identifies Host Factors

883 Essential for Influenza Virus Replication. *Cell Rep* **23**:596–607.
884 doi:10.1016/j.celrep.2018.03.045
885 Huch M, Gehart H, van Boxtel R, Hamer K, Blokzijl F, Verstegen MMA, Ellis E, van Wenum M,
886 Fuchs SA, de Ligt J, van de Wetering M, Sasaki N, Boers SJ, Kemperman H, de Jonge J,
887 Ijzermans JNM, Nieuwenhuis EES, Hoekstra R, Strom S, Vries RRG, van der Laan LJW,
888 Cuppen E, Clevers H. 2015. Long-term culture of genome-stable bipotent stem cells from
889 adult human liver. *Cell* **160**:299–312. doi:10.1016/j.cell.2014.11.050
890 Hyrina A, Jones C, Chen D, Clarkson S, Cochran N, Feucht P, Hoffman G, Lindeman A, Russ C,
891 Sigoillot F, Tsang T, Uehara K, Xie L, Ganem D, Holdorf M. 2019. A Genome-wide CRISPR
892 Screen Identifies ZCCHC14 as a Host Factor Required for Hepatitis B Surface Antigen
893 Production. *Cell Rep* **29**:2970-2978.e6. doi:10.1016/j.celrep.2019.10.113
894 Jacobsen KH. 2018. Globalization and the Changing Epidemiology of Hepatitis A Virus. *Cold*
895 *Spring Harb Perspect Med* **8**:a031716. doi:10.1101/cshperspect.a031716
896 Jiang X, Kanda T, Wu S, Nakamoto S, Saito K, Shirasawa H, Kiyohara T, Ishii K, Wakita T,
897 Okamoto H, Yokosuka O. 2014. Suppression of La Antigen Exerts Potential Antiviral
898 Effects against Hepatitis A Virus. *PLOS ONE* **9**:e101993.
899 doi:10.1371/journal.pone.0101993
900 Kang SH, Kim GR, Seong M, Baek SH, Seol JH, Bang OS, Ovaa H, Tatsumi K, Komatsu M, Tanaka
901 K, Chung CH. 2007. Two novel ubiquitin-fold modifier 1 (Ufm1)-specific proteases, UfSP1
902 and UfSP2. *J Biol Chem* **282**:5256–5262. doi:10.1074/jbc.M610590200
903 Kaplan G, Totsuka A, Thompson P, Akatsuka T, Moritsugu Y, Feinstone SM. 1996. Identification
904 of a surface glycoprotein on African green monkey kidney cells as a receptor for
905 hepatitis A virus. *EMBO J* **15**:4282–4296.
906 Kempf BJ, Kelly MM, Springer CL, Peersen OB, Barton DJ. 2013. Structural features of a
907 picornavirus polymerase involved in the polyadenylation of viral RNA. *J Virol* **87**:5629–
908 5644. doi:10.1128/JVI.02590-12
909 Ko C, Chakraborty A, Chou W-M, Hasreiter J, Wettengel JM, Stadler D, Bester R, Asen T, Zhang
910 K, Wisskirchen K, McKeating JA, Ryu W-S, Protzer U. 2018. Hepatitis B virus genome
911 recycling and de novo secondary infection events maintain stable cccDNA levels. *J*
912 *Hepatol* **69**:1231–1241. doi:10.1016/j.jhep.2018.08.012
913 Komatsu M, Chiba T, Tatsumi K, Iemura S, Tanida I, Okazaki N, Ueno T, Kominami E, Natsume T,
914 Tanaka K. 2004. A novel protein-conjugating system for Ufm1, a ubiquitin-fold modifier.
915 *EMBO J* **23**:1977–1986. doi:10.1038/sj.emboj.7600205
916 Ladner SK, Otto MJ, Barker CS, Zaifert K, Wang GH, Guo JT, Seeger C, King RW. 1997. Inducible
917 expression of human hepatitis B virus (HBV) in stably transfected hepatoblastoma cells:
918 a novel system for screening potential inhibitors of HBV replication. *Antimicrob Agents*
919 *Chemother* **41**:1715–1720.
920 Landry DM, Hertz MI, Thompson SR. 2009. RPS25 is essential for translation initiation by the
921 Dicistroviridae and hepatitis C viral IRESs. *Genes Dev* **23**:2753–2764.
922 doi:10.1101/gad.1832209
923 Lemon SM, Murphy PC, Shields PA, Ping LH, Feinstone SM, Cromeans T, Jansen RW. 1991.
924 Antigenic and genetic variation in cytopathic hepatitis A virus variants arising during
925 persistent infection: evidence for genetic recombination. *J Virol* **65**:2056–2065.

926 Li W, Xu H, Xiao T, Cong L, Love MI, Zhang F, Irizarry RA, Liu JS, Brown M, Liu XS. 2014. MAGeCK
927 enables robust identification of essential genes from genome-scale CRISPR/Cas9
928 knockout screens. *Genome Biol* **15**:554. doi:10.1186/s13059-014-0554-4
929 Lim J, Kim D, Lee Y-S, Ha M, Lee M, Yeo J, Chang H, Song J, Ahn K, Kim VN. 2018. Mixed tailing
930 by TENT4A and TENT4B shields mRNA from rapid deadenylation. *Science* **361**:701–704.
931 doi:10.1126/science.aam5794
932 Lubas M, Christensen MS, Kristiansen MS, Domanski M, Falkenby LG, Lykke-Andersen S,
933 Andersen JS, Dziembowski A, Jensen TH. 2011. Interaction Profiling Identifies the Human
934 Nuclear Exosome Targeting Complex. *Mol Cell* **43**:624–637.
935 doi:10.1016/j.molcel.2011.06.028
936 Luo B, Cheung HW, Subramanian A, Sharifnia T, Okamoto M, Yang X, Hinkle G, Boehm JS,
937 Beroukhim R, Weir BA, Mermel C, Barbie DA, Awad T, Zhou X, Nguyen T, Piqani B, Li C,
938 Golub TR, Meyerson M, Hacohen N, Hahn WC, Lander ES, Sabatini DM, Root DE. 2008.
939 Highly parallel identification of essential genes in cancer cells. *Proc Natl Acad Sci U S A*
940 **105**:20380–20385. doi:10.1073/pnas.0810485105
941 Majzoub K, Hafirassou ML, Meignin C, Goto A, Marzi S, Fedorova A, Verdier Y, Vinh J, Hoffmann
942 JA, Martin F, Baumert TF, Schuster C, Imler J-L. 2014. RACK1 controls IRES-mediated
943 translation of viruses. *Cell* **159**:1086–1095. doi:10.1016/j.cell.2014.10.041
944 Marceau CD, Puschnik AS, Majzoub K, Ooi YS, Brewer SM, Fuchs G, Swaminathan K, Mata MA,
945 Elias JE, Sarnow P, Carette JE. 2016. Genetic dissection of Flaviviridae host factors
946 through genome-scale CRISPR screens. *Nature* **535**:159–163. doi:10.1038/nature18631
947 McKnight KL, Lemon SM. 2018. Hepatitis A Virus Genome Organization and Replication
948 Strategy. *Cold Spring Harb Perspect Med* a033480. doi:10.1101/cshperspect.a033480
949 Mueller H, Lopez A, Tropberger P, Wildum S, Schmaler J, Pedersen L, Han X, Wang Y, Ottosen S,
950 Yang S, Young JAT, Javanbakht H. 2019. PAPD5/7 Are Host Factors That Are Required for
951 Hepatitis B Virus RNA Stabilization. *Hepatology* **69**:1398–1411. doi:10.1002/hep.30329
952 Mueller H, Wildum S, Luangsay S, Walther J, Lopez A, Tropberger P, Ottaviani G, Lu W, Parrott
953 NJ, Zhang JD, Schmucki R, Racek T, Hoflack J-C, Kueng E, Point F, Zhou X, Steiner G,
954 Lütgehetmann M, Rapp G, Volz T, Dandri M, Yang S, Young JAT, Javanbakht H. 2018. A
955 novel orally available small molecule that inhibits hepatitis B virus expression. *J Hepatol*
956 **68**:412–420. doi:10.1016/j.jhep.2017.10.014
957 Nousch M, Yeroslaviz A, Habermann B, Eckmann CR. 2014. The cytoplasmic poly(A)
958 polymerases GLD-2 and GLD-4 promote general gene expression via distinct
959 mechanisms. *Nucleic Acids Res* **42**:11622–11633. doi:10.1093/nar/gku838
960 Pestova TV, Hellen CU, Shatsky IN. 1996. Canonical eukaryotic initiation factors determine
961 initiation of translation by internal ribosomal entry. *Mol Cell Biol* **16**:6859–6869.
962 doi:10.1128/MCB.16.12.6859
963 Rammelt C, Bilen B, Zavolan M, Keller W. 2011. PAPD5, a noncanonical poly(A) polymerase with
964 an unusual RNA-binding motif. *RNA* **17**:1737–1746. doi:10.1261/rna.2787011
965 Rivera-Serrano EE, González-López O, Das A, Lemon SM. 2019. Cellular entry and uncoating of
966 naked and quasi-enveloped human hepatoviruses. *eLife* **8**:e43983.
967 doi:10.7554/eLife.43983

968 Shcherbik N, Wang M, Lapik YR, Srivastava L, Pestov DG. 2010. Polyadenylation and degradation
969 of incomplete RNA polymerase I transcripts in mammalian cells. *EMBO Rep* **11**:106–111.
970 doi:10.1038/embor.2009.271
971 Shin J, Paek KY, Ivshina M, Stackpole EE, Richter JD. 2017. Essential role for non-canonical
972 poly(A) polymerase GLD4 in cytoplasmic polyadenylation and carbohydrate metabolism.
973 *Nucleic Acids Res* **45**:6793–6804. doi:10.1093/nar/gkx239
974 Shukla P, Nguyen HT, Faulk K, Mather K, Torian U, Engle RE, Emerson SU. 2012. Adaptation of a
975 genotype 3 hepatitis E virus to efficient growth in cell culture depends on an inserted
976 human gene segment acquired by recombination. *J Virol* **86**:5697–5707.
977 doi:10.1128/JVI.00146-12
978 Spector DH, Baltimore D. 1975. Polyadenylic acid on poliovirus RNA: IV. Poly(U) in replicative
979 intermediate and double-stranded RNA. *Virology* **67**:498–505. doi:10.1016/0042-
980 6822(75)90450-X
981 Steil BP, Kempf BJ, Barton DJ. 2010. Poly(A) at the 3' End of Positive-Strand RNA and VPg-Linked
982 Poly(U) at the 5' End of Negative-Strand RNA Are Reciprocal Templates during
983 Replication of Poliovirus RNA. *J Virol* **84**:2843–2858. doi:10.1128/JVI.02620-08
984 Tatsumi K, Sou Y, Tada N, Nakamura E, Iemura S, Natsume T, Kang SH, Chung CH, Kasahara M,
985 Kominami E, Yamamoto M, Tanaka K, Komatsu M. 2010. A novel type of E3 ligase for the
986 Ufm1 conjugation system. *J Biol Chem* **285**:5417–5427. doi:10.1074/jbc.M109.036814
987 Vaňáčová Š, Wolf J, Martin G, Blank D, Dettwiler S, Friedlein A, Langen H, Keith G, Keller W.
988 2005. A New Yeast Poly(A) Polymerase Complex Involved in RNA Quality Control. *PLOS*
989 *Biol* **3**:e189. doi:10.1371/journal.pbio.0030189
990 Votteler J, Sundquist WI. 2013. Virus Budding and the ESCRT Pathway. *Cell Host Microbe*
991 **14**:232–241. doi:10.1016/j.chom.2013.08.012
992 Walczak CP, Leto DE, Zhang L, Riepe C, Muller RY, DaRosa PA, Ingolia NT, Elias JE, Kopito RR.
993 2019. Ribosomal protein RPL26 is the principal target of UFMylation. *Proc Natl Acad Sci*
994 *U S A* **116**:1299–1308. doi:10.1073/pnas.1816202116
995 Wang L, Xu Y, Rogers H, Saidi L, Noguchi CT, Li H, Yewdell JW, Guydosh NR, Ye Y. 2019.
996 UFMylation of RPL26 links translocation-associated quality control to endoplasmic
997 reticulum protein homeostasis. *Cell Res*. doi:10.1038/s41422-019-0236-6
998 Warkocki Z, Liudkovska V, Gewartowska O, Mroczek S, Dziembowski A. 2018. Terminal
999 nucleotidyl transferases (TENTs) in mammalian RNA metabolism. *Philos Trans R Soc B*
1000 *Biol Sci* **373**:20180162. doi:10.1098/rstb.2018.0162
1001 Wu J, Lei G, Mei M, Tang Y, Li H. 2010. A novel C53/LZAP-interacting protein regulates stability
1002 of C53/LZAP and DDRGK domain-containing Protein 1 (DDRGK1) and modulates NF-
1003 kappaB signaling. *J Biol Chem* **285**:15126–15136. doi:10.1074/jbc.M110.110619
1004 Zhang R, Miner JJ, Gorman MJ, Rausch K, Ramage H, White JP, Zuiani A, Zhang P, Fernandez E,
1005 Zhang Q, Dowd KA, Pierson TC, Cherry S, Diamond MS. 2016. A CRISPR screen defines a
1006 signal peptide processing pathway required by flaviviruses. *Nature* **535**:164–168.
1007 doi:10.1038/nature18625
1008